AI-Based Shear Capacity of FRP-Reinforced Concrete Deep Beams without Stirrups

Mohammad AlHamaydeh [1], George Markou [2], Nikos Bakas[3], and Manolis Papadrakakis [4]

[1] Corresponding author: Professor, Department of Civil Engineering, College of Engineering, American University of Sharjah, Sharjah, PO Box 26666, UAE; malhamaydeh@aus.edu , ORCID ID: 0000-0002-5004-0778.

[2] Associate Professor, Department of Civil Engineering, Faculty of Engineering, Built Environment and Information Technology, University of Pretoria, South Africa, george.markou@up.ac.za

[3] Associate Research Scientist, The Cyprus Institute, Cyprus, n.bakas@cyi.ac.cy

[4] Professor, Institute of Structural Analysis & Antiseismic Research, National Technical University of Athens, Zografou Campus, Athens, Greece, mpapadra@central.ntua.gr

ABSTRACT

The presented work utilizes Artificial Intelligence (AI) algorithms, to model and interpret the behavior of the fiber reinforced polymer (FRP)-reinforced concrete deep beams without stirrups. This is done by first running an extensive nonlinear finite element analysis (NLFEA) investigation, spanning across the practical ranges of the different input parameters. The FEA modeling is meticulously validated against published experimental results. A total of 93 different models representing a multitude of possible FRP-reinforced deep beam designs are rigorously analyzed. The results are then utilized in building an AI-model that describes the shear capacity for FRP-reinforced deep beams. The study investigates the effect of several factors on the shear capacity and identifies the vital parameters to be used for further model development. Additionally, the developed AI-model is benchmarked against several design standards for blind predictions on new unseen data and design codes, namely: the EC, ACI 440.1R-15, and the modified ACI 440.1R-15 (for size effect). The AI-model demonstrated superior generalization on the blind prediction dataset in comparison to the design codes.

Keywords: Nonlinear FEA, Artificial Intelligence, FRP, Deep Beams without Stirrups.

1 Introduction and Background

The past century has witnessed significant advancements in steel-reinforced concrete structures. However, a number of structural systems of this type still pose major challenges due to the strenuous environments they are subjected to. Corrosion of steel reinforcements in reinforced concrete (RC) infrastructure constitutes the primary cause of concrete deterioration, which leads to costly repairs and shorter service life. To alleviate the high repair cost, different types of reinforcement have been used, such as stainless, epoxy coated, and galvanized steel. Fiber-reinforced polymers (FRPs) have been recently proposed as an alternative to steel reinforcement due to their advantages when compared to conventional steel reinforcement bars [1]–[6]. FRP reinforcement is characterized by its high immunity to corrosion, which increases the service life of the concrete and reduces its repair expenses [7]–[9].

In addition to the above, FRP bars are non-corrosive, non-conductive, magnetically inert, and have a high strength-to-weight ratio. Their mechanical properties are also considerably enhanced compared to those of steel. FRP bars have a high tensile strength [10], which contributes to the flexural capacity of the reinforced concrete elements and causes them to have a high strength-to-weight ratio which facilitates handling and installing them in concrete [3]. However, the axial rigidity of FRP bars is usually lower than that of steel bars and large transverse deformations are expected for FRP-reinforced members. FRP is also characterized by a low modulus of elasticity, which adversely affects aggregate interlock and dowel action, leading to larger crack widths, greater deformations, and reduced shear strength in the structural elements [11]–[14]. Large deformations lead to wider flexural and shear cracks, hence reducing the shear capacity of slender-RC beams with no web reinforcement due to weak interlocking of aggregates and decreased contribution of dowel action to shear strength [15], [16].

The shear strength of a concrete beam is directly proportional to its shear span-to-effective depth ratio (a/d). Based on this criterion, various codes such as the ACI 318M-14 [17] and the CSA A23.3-14 [18] divide beams into two categories, deep beams and slender beams. FRP-reinforced deep beams with shear span-to-depth ratio $a/d \leq 2.0$ are known to have larger shear capacity than those of FRP-reinforced slender beams with $a/d > 2.0$ [12], [16], [19]. Other codes, such as the Eurocode 2 [20], adopt a more conservative definition, whereby deep beams are defined as the beams with a clear span-to-depth ratio (l/h) of less than 3.0. Unlike slender beams, loads supported by deep beams are transferred directly to supports through diagonal compression struts creating compression stresses rather than shear stresses. Such a mechanism is referred to as the arch action, which describes the direct transfer of shear forces from the loading points to the supports, through the buildup of compressive stresses caused by the realignment of internal forces after cracking [21]. This results in the formation of compression struts between the loading points and the supports, as opposed to the development of shear stresses in slender beams with tension ties configured by the longitudinal reinforcement acting as arch ribs in compression. According to ACI 318-14, a deep beam is defined as a beam with a clear span (Lo) to height (h) ratio, $Lo/h < 4.0$ or with a shear span (a) to height (h) ratio $a/h < 2.0$, while other codes define deep concrete beam as a beam with a shear span (a) to depth (d) ratio, $a/d < 2.5$. Deep beams are completely dominated by a disturbed region (D region) characterized by a non-linear strain-stress distribution. Thus, the sectional model used to evaluate the shear strength of slender beams is not applicable [22]. Instead, available codes allow the use of the strut-and-tie model (STM) method, among others, to design deep beams and estimate their capacities. The shear capacity is of great importance for deep beams because their failure is generally caused by shear due to the non-linear distribution of strain [23]. The large depths present in deep beams cause the stress-strain relationship to deviate from its linearity and in the nonlinear range from its parabolic curve with a clearly defined ultimate stress leading to shear failure [23].

The STM method assumes that the applied load is directly transmitted to the supports by in-plane compression through an inclined strut rather than a shearing force, thus significantly overestimating the beam's shear strength. The shear strength of concrete deep beams is generally governed by the strength of the inclined concrete strut near the bottom node [24]. According to the modified compression field theory, the critically low strength of the inclined concrete strut is attributed to the presence of transverse tensile strain induced by the strain developed in the longitudinal steel reinforcement [25]. Existing codes account for this phenomenon by applying a reduction factor to the strength of the inclined concrete struts.

The shear strength of slender beams longitudinally reinforced with FRP bars has been studied intensively over the past decades. Thus, multiple design formulas and guidelines have been made available in codes, such as the ACI 440.1R-06 [10], the CSA S806 [26], and the Concrete Society Technical Report [27]. Studies have shown that FRP-reinforced slender beams exhibit a lower shear strength compared to equivalent steel-reinforced beams. The drop in shear strength is attributed to the lower modulus of elasticity and poorer bonding characteristics of FRP [12], [28], [29].

Multiple research studies have been conducted on slender concrete beams comparing the shear behavior of specimens reinforced with steel rebars and specimens reinforced with FRP rebars. It was concluded that the two types of reinforcement yielded considerably different shear behaviors [30]–[31]. El-Sayed et al. [19], [31] compared slender concrete beams reinforced with carbon fiber reinforced polymer (CFRP), glass fiber reinforced polymer (GFRP), and conventional steel, respectively. The study concluded that steel-reinforced beams had the highest shear strength, confirming that shear capacity is generally proportional to the rebars' modulus of elasticity. Results of this study also featured a proposed modification to the shear design equation of FRP-reinforced beams available in ACI 440.1R03, which was, however, deemed overly conservative. In a similar study, ten concrete beams reinforced with GFRP rebars and stirrups were tested under four-point loading [32]. The outcome of this study was a new design approach to compute the shear capacity of concrete beams reinforced with FRP stirrups [32]. Furthermore, other studies on deep beams have shown that deep beams as well exhibit a lower shear capacity when compared to their steel-reinforced counterparts, as a result of the low modulus of elasticity characteristic of FRP, which leads to wider shear cracks and larger transverse tensile strains, reducing the shear strength of the inclined concrete strut and ultimately reducing the overall shear capacity of the concrete beam [19], [33], [34].

Due to their high shear resistance, deep beams are commonly used as transfer girders in high-rise buildings and bridges, shear walls, and pile caps. In most cases, they are exposed to aggressive environments and using FRP bars to reinforce such members can reduce the rehabilitation cost and enhance their service life. Previously conducted studies [30]–[31], showed that the shear behavior of FRP-RC slender beams differs from that of steel-reinforced slender beams. However, the shear behavior of deep RC members, in general, is still unclear and further research in this scientific topic is needed. Experimental studies on the shear behavior of FRP-reinforced concrete deep members, in particular, are limited and more comprehensive studies to investigate the shear behavior of such members are needed. More importantly, there are still no specific design codes for FRP-RC beams in general. While some codes, such as the American Concrete Institute, permit the use of the strut-and-tie model (STM) analysis [17], others, like the Canadian Standards Association, do not [35]. Current guidelines recommend using slightly modified shear design equations originally developed for steel-reinforced slender beams. Such equations are not applicable for the design of either steel or FRP-RC deep members and current standards recommend the use of the strut-and-tie method to determine the shear capacity of beams with a/h < 2.0. It is, therefore, important to investigate the performance in shear of FRP-RC deep beams and compare it to that of steel-reinforced concrete deep beams to explore differences in their shear behavior and mode of failure. Such differences should be considered when developing new or revised shear design rules to determine the shear capacity of FRP concrete deep beams [36].

Building codes, such as the ACI 440.1R-06 [10], the CSA S806 [26], and the Concrete Society Technical Report [27], dictate some constraints on the values of the design variables such as:

$$\frac{L}{a} \geq 2.1 \tag{1}$$

$$\frac{b}{h} \leq 0 \tag{2}$$

$$1.5 \leq \frac{L}{h} \leq 4 \tag{3}$$

Since some of the aforementioned variables are dependent on each other, as shown in equations 1-3, some of them will be combined into a ratio-independent variable. Five variables will be investigated in this paper with different values (levels), as shown in Section 3.

To investigate the effect of each variable and model the force-deflection behavior, a statistical analysis is performed on the numerically generated database. The numerically obtained database was further analyzed to establish conceptual information about the interactions among the independent variables and the maximum capacity force. Accordingly, a nonlinear prediction model was developed by implementing a variety of machine learning (ML) algorithms. The implemented methodology is based on a recent study for the precise implementation of ML algorithms to RC datasets. In particular, as demonstrated in [37], [38], artificial intelligence (AI) algorithms were found able to predict RC strength and dynamic response characteristics without training on experimental data. The prediction accuracy was satisfying, by exhibiting errors lower than that obtained from Building Codes [38]. The same procedure was implemented in this work for FRP-RC deep beams, as presented in Section 4 Statistical Analysis.

Several researchers have investigated the mechanical properties, mainly the shear behavior, of deep beams with FRP reinforcement composed of common fibers such as glass (GFRP), carbon (CFRP), and basalt (BFRP). An early research study by Omeman et al. [14] investigated the shear behavior of CFRP-reinforced deep beams with no web reinforcement. They compared CFRP-reinforced deep beams to steel reinforced deep beams in terms of shear strength, deflection, and mode of failure. Shear strength of CFRP-reinforced deep beams was found to be higher than that of steel-reinforced deep beams due to the improved arch action mechanism that stems from the higher tensile strength of CFRP bars. Additional findings revealed that an increase in shear strength was achieved by increasing the effective depth, reinforcement ratio, and concrete compressive strength, while decreasing a/d. Meanwhile, deflection was decreased by increasing the effective depth and concrete compressive strength. Reinforcement ratio did not have an effect on deflection. The most common mode of failure in deep beams was shear failure for both types of reinforcement. However, due to lower modulus of elasticity, CFRP-reinforced deep beams had wider cracks than other conventional deep beams. Researchers also concluded that the STM needed modification by calibration in order to account for deficiencies that occur when it is applied to deep beams with FRP reinforcement [14].

The external application of FRP to enhance the shear capacity of conventionally reinforced concrete deep beams has been studied extensively. Islam et al. [39], tested deep beams strengthened with CFRP strips, wraps, and grids until failure. The results of the study confirmed an enhanced shear capacity due to external FRP strengthening. However, the study failed to fully capture improvements in the specimens' load carrying capacity due to inherent flaws in the STM method. A similar study was conducted in [40], in which CFRP composite sheets were used to strengthen concrete deep beams with two square openings. It was concluded that CFRP strengthening around the openings enhanced stiffness and shear capacity. This study also presented a comparison of experimental with analytical results, based on proposed methods in existing literature, where the shear capacity of CFRP strengthened deep beams with openings can be accurately predicted. Using finite element analysis, Hassan et al. [41], also confirmed about the improved shear capacity due to FRP strengthening in concrete beams with openings.

One of the limited research works on deep beams with internal FRP reinforcement and no web reinforcement, is an experimental study conducted by El-Sayed et al. [42], in which ten full-scale deep beams were tested under four-point loading. One half of the specimens were reinforced with GFRP rebars, and the other were reinforced with CFRP rebars. Test parameters included the reinforcement ratio, which varied from 0.78% to 1.71%, and the shear span-to-depth (a/d) ratio, which varied from 0.92% to 1.69%. The results revealed that by increasing the reinforcement ratio, the shear capacity for both types of reinforcement increased. Moreover, decreasing the a/d ratio resulted in a significant increase in the ultimate shear strength. However, a less significant increase was observed in the specimens' inclined shear strength.

Kim et al. [34], conducted a similar experiment, in which 15 deep beam specimens with no web reinforcement were tested under two-point loading. The objectives of the study were the investigation of the effects of various parameters on the shear capacity of deep beams, as well as to propose an effectiveness factor for STM analysis. The parameters investigated were the reinforcement type (steel, CFRP, and Aramid FRP, respectively), the reinforcement ratio, the a/d ratio, and the effective beam depth. It was noted that decreasing the a/d ratio, increasing the reinforcement ratio, and increasing the effective depth increased the shear capacity of the specimens. In addition, an effectiveness factor was proposed to better estimate the shear capacity of FRP-reinforced deep beams using STM analysis.

Another study conducted by Farghaly and Benmokrane [1] investigated the factors affecting the capacity and deflection of deep beams with CFRP and GFRP reinforcement using STM methods that adhere to the ACI-318 and CSA-S806 code provisions. It was confirmed that the capacities were predominantly affected by the reinforcement ratio and the concrete compressive strength, but they were not significantly influenced by the reinforcement type [1]. However, Mohamed et al. [43] assessed both ACI and CSA STM's and concluded that the efficiency factor of ACI-318 overestimated the shear strength while the efficiency factor of CSA-S806 underestimated the capacity. For this reason, many research efforts were directed towards making variations to conventional STM methods in order to best fit the behavior of FRP-reinforced deep beams. Chen et al. [44] proposed a cracking STM (CSTM) in order to accurately model the shear behavior of steel reinforced deep beam, taking into account the effect of diagonal cracks. The CSTM was recently modified and used by Chen et al. [45] to be applicable to FRP-reinforced deep beams. It was proven that the modified CSTM correctly predicted the shear capacity of the beams and the main factors influencing it.

Similarly, Andermatt and Lubell [46], examined the effects of three parameters: a/d, effective depth, and concrete compressive strength on GFRP-reinforced deep beams. The findings agreed with previous studies highlighting that an increase in shear capacity was obtained by decreasing a/d. They used ACI 318-08 and CSA S806-02 STM's to study the capacity. CSA S806-02 provided more accurate predictions than those of ACI 318-08 STM [46]. While such studies tested the effects of multiple factors, Tomlinson and Fam [13] conducted a more specific investigation focused on the effect of reinforcement ratio on deep beams reinforced with BFRP bars with no stirrups. The results revealed that increasing the reinforcement ratio by 2.15 times generated a 54 percent increase in the shear strength. This was due to a higher rebar dowel action and a stronger interlock between the aggregates [13].

Recognizing the above design limitations, this study numerically and analytically investigates the shear behavior of FRP-RC deep beams and provides the much-needed database to help develop more detailed and reliable shear design recommendations. It will also provide a thorough investigation of the effect of basic shear design parameters on the shear capacity of FRP-RC deep beams, thus, contributing to the understanding of different aspects involved in the design and analysis of such structural members.

In another study, Andermatt and Lubell [33] tested 12 full-scale deep beams reinforced with GFRP, to investigate their shear behavior and modes of failure. Deflections were recorded using linear variable differential transformers (LVDTs) and strains were recorded using strain gauges. Measurements of strain, crack widths and observations of crack orientations, demonstrated the arch mechanism characteristic of concrete deep beams. It was found that the efficiency of the arch mechanism decreased with increase in a/d ratio, as a consequence of reduced reserve capacity with reduced inclined cracking. In a different study of Andermatt and Lubell [47], investigated five sectional shear design models, which aim to predict the shear strength of FRP-reinforced deep beams. The study revealed that none of the examined models, including the STM approach modified for FRP-reinforced beams in ACI 318-08, accurately captured the arch mechanism, thus underestimating the increase in shear capacity with a decreasing a/d ratio. Furthermore, through a nonlinear finite element analysis, it was deduced that deflection, rather than strength, is the governing factor in the design of FRP-reinforced concrete deep beams [48]. However, further investigation is required to account for factors like concrete creep, concrete shrinkage, and fire exposure [49].

According to the international literature, it is commonly accepted that further investigation is required in developing accurate and objective design formulae for the prediction of the shear capacity of deep beams reinforced with FRP bars. To achieve this objective, the authors believe that a multi-disciplinary approach has to be considered that will involve both numerical and experimental activities. More specifically, AI-Based models are developed to accurately predict the shear capacity of deep FRP-RC beams without stirrups. The AI-based modeling is developed primarily from an extensive numerical investigation campaign, utilizing high-fidelity numerical approaches. The response of a 3D detailed model simulating the structural behavior of 93 GFRP-reinforced concrete deep beams without shear reinforcement is utilized herein. The ultimate shear capacity obtained from the nonlinear finite element analysis (NLFEA), serves as the input for the AI modeling effort. The numerical results are augmented with a supplemental set of experimental results from nine beams from a previous publication [50]. Section 3 of this article sheds light on the intricate details of the NLFEA implementation. Subsequently, Section 4 lays out the groundwork for the AI-modeling techniques used. Furthermore, Section 5 demonstrates the predictive and generalization capabilities on the proposed AI-based model. Concluding remarks are presented in Section 5.

2 Research Significance

This research is believed to provide profound insights into the shear capacity of FRP-reinforced deep deems without shear reinforcement. To the best of the authors' knowledge, this type of AI modeling has never been attempted in the available literature. The presented model is capable of accurately predicting the shear capacity for beams with all currently available FRP reinforcement [GFRP, CFRP, AFRP, BFRP]. The model is developed using a hybrid dataset of experimentally obtained results in combination with high-fidelity numerical modeling approach via the widely accepted smeared crack approach. While the blind predictions are made for experimentally obtained data, demonstrating the model's capability to accurately capture the physical phenomena. Moreover, the presented model can be further tweaked and refined with new data as it becomes available in the literature. It is worth noting that in blind predictions for experimental testing data, the presented model has consistently outperformed design codes and standards. As such, it provides a convenient closed-form design equation for structural designers upon potential adoption into codes and standards.

3 Nonlinear Finite Element Analysis (NLFEA) Investigation

An excessive NLFEA investigation was performed in this research work, which was based on the meticulously validated finite element (FE) modeling of RC structures [50], where GFRP concrete deep beams without shear reinforcement were studied through the use of ReConAn FEA [51]. The purpose of this study was to derive FE models that are capable of capturing the experimental results (of nine four-point bending tests) with high levels of accuracy and computational efficiency. In achieving this objective, the 20-noded hexahedral element was used for the discretization of the concrete domain, while the concrete material was modeled through a 3D concrete constitutive material model that assumes a brittle behavior after the occurrence of a macro-crack at a Gauss point within the concrete hexahedral finite element (see [52] and for the most recent advancement of the method [53][54]). The GFRP bars were modeled as embedded 2-noded rod elements [50] by assuming full bond conditions with concrete, while the material model used in simulating the stress-strain relationship for the GFRP bar material assumed linear behavior until complete failure by both tension and compression.

From the numerical investigation performed by Markou and AlHamaydeh [50], it was revealed that the developed 3D detailed model was capable in capturing the mechanical behavior of all nine GFRP concrete deep beams with a 2.47% overall deviation from the experimental data in predicting the ultimate load capacity and a 10.36% deviation in predicting the ultimate deflection. In Fig. 1, specimen B5 is presented where the deformed shape and the crack patterns is depicted according to the FE analysis in [50].

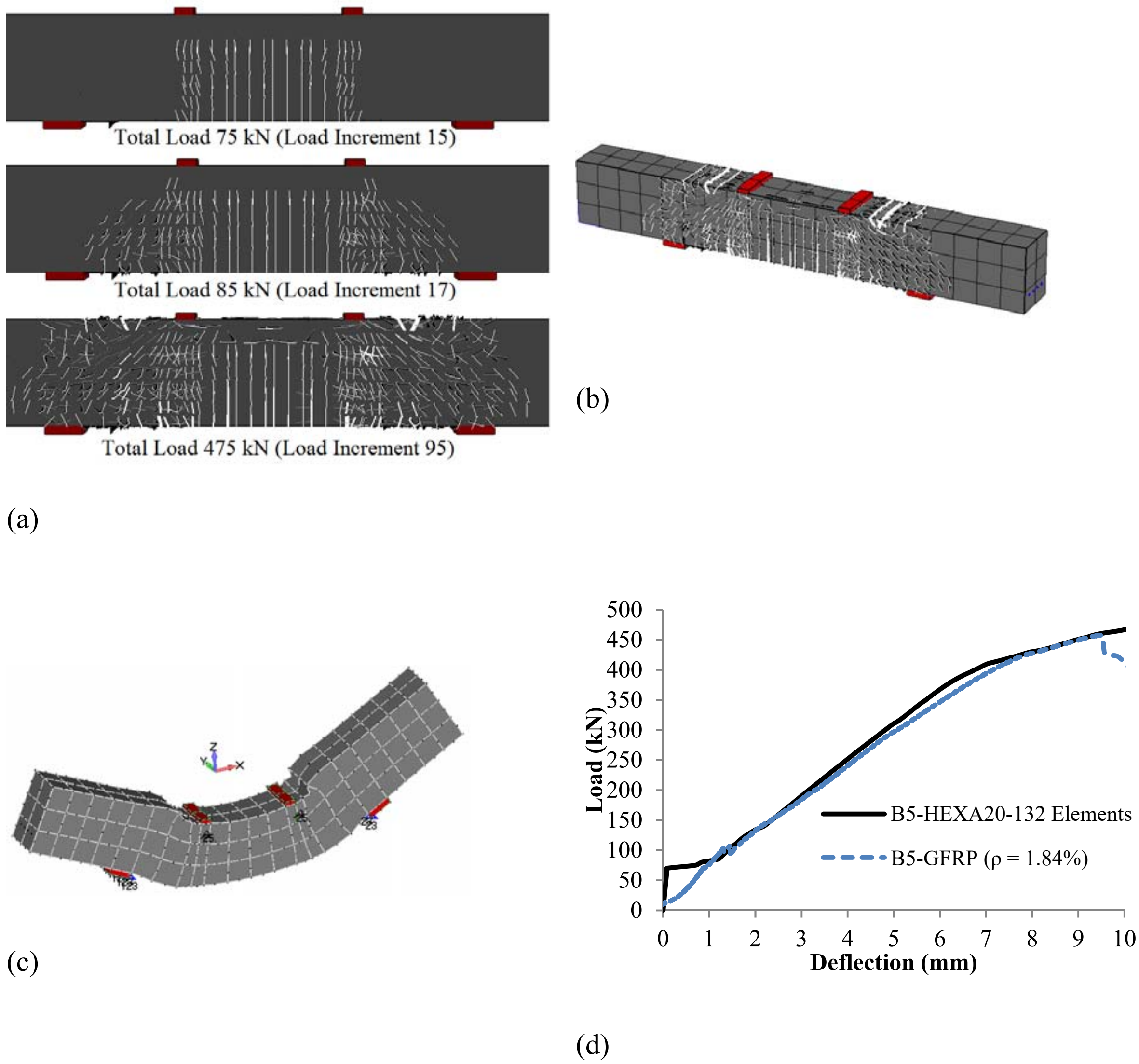

Figure 1. Beam specimen B5. (a) Crack patterns at different load increments, (b) 3D view of the crack pattern prior to failure, (c) Deformed shape prior to failure (scaled by 100) and (d) Load-deflection curves. [50]

As can be seen in Fig. 1, the load-deflection curves of the experimental and numerical results are in good agreement. It must be noted here that from the numerical investigation performed in [50], it was found that the optimum value of the remaining shear stiffness β after a crack occurs at a Gauss point, was 3.16%, which is also the unified value adopted in the numerical investigation performed herein. The FE model used in the numerical tests of this study is presented subsequently.

3.1 NLFEA Model Description

As it was mentioned earlier, 93 FE models were implemented (see Table 1) to study the structural behavior of concrete deep beams that were reinforced with three different FRP rebar material types

(Glass, Carbon, and Aramid). Appropriate values of the material properties were selected to capture low, baseline and high levels for all input parameters, to be implemented in the FE models (see Table 2 for adopted values). The deep beams were also studied for different geometries and material properties, as depicted in Tables 1-2. Appendix A shows the dataset of the beams that were used to train and test the proposed AI-model.

Table 1: FE Mesh Groups of the 93 deep beam models and the experimentally tested beams.

Group	Dimensions b x h x L (mm x mm x mm)	Beam Model Designation	Total Number of Beams
1	200 x 800 x 1600	1 – 8	8
2	400 x 800 x 1600	9 – 16	8
3	200 x 475 x 2024	17 – 24	8
4	400 x 810 x 3400	25 – 32	8
5	200 x 1061 x 3636	33	1
6	400 x 1061 x 3636	34	1
7	300 x 1061 x 3636	35 – 42	8
8	300 x 675 x 2833	43	1
9	250 x 1731 x 3181	44 – 59	16
10	250 x 1038 x 3544	60 – 67	8
11	350 x 1038 x 3544	68 – 75	8
12	350 x 1731 x 3181	76 – 84	9
*13	200 x 300 x 1000 200 x 350 x 1000 200 x 400 x 1000	85 – 93	9
min-max b (mm)	200-400	-	-
min-max d (mm)	300-1731	-	-

min-max L (mm)	1000-3636	-	-

* Experimentally and numerically tested specimens [50, 55] — Total **93**

Table 2: Reinforced beam design variables

Variable	Unit	Low level	Base line level	High Level
Beam width (b)	mm	200	300	400
Concrete properties (E_c/F_c)		701	794	940
Reinforced material properties (E_c/F_c)		71	73	75
Shear span (a/h)		0.5	1.25	2
Reinforced ratio (ρ)	%	0.2991	0.7854	2.595

A uniform hexahedral FE mesh size was used to discretize each beam model with a 10 cm average edge size. This was also the FE mesh size adopted in the parametric investigation presented in [50], where a mesh sensitivity analysis was also performed. To capture the exact geometry of the beam, the 20-noded hexahedral FE dimensions were modified according to the specimen's geometry. Fig. 2 illustrates the 13 different model groups developed for the needs of this numerical investigation. It must be noted here that the reinforcement in all beam models was discretized through 4 rebars, thus the corresponding diameter resulted according to the reinforcement ratio adopted for each deep beam (see Table 2). Table 1 shows the overall mesh dimensions of each group of beams and the corresponding number of beam models that are included within each group.

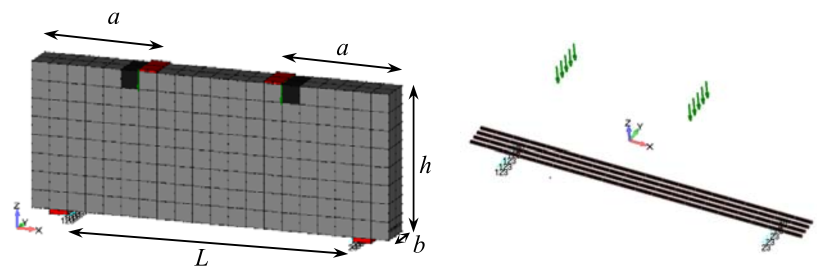

Group 1 - Beam 1 (Left) 20-noded hexahedral mesh and (Right) Embedded rebar rod elements.

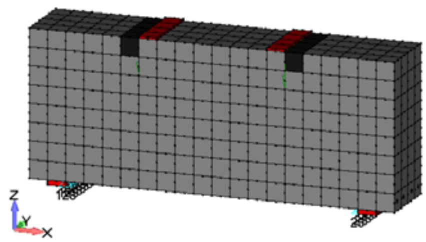

Group 2

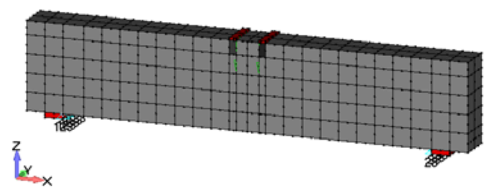

Group 3

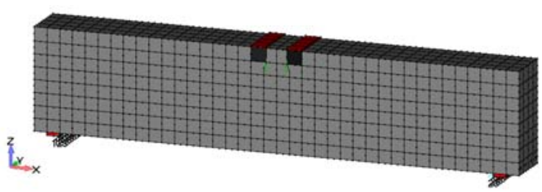

Group 4

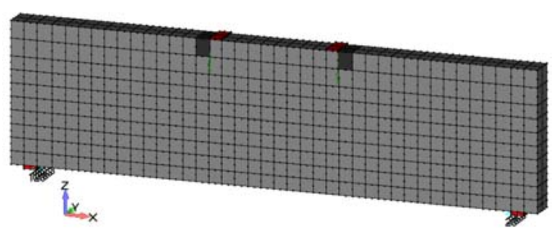

Group 5

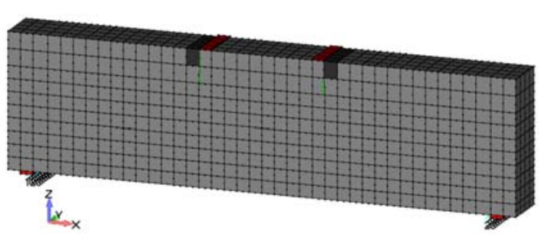

Group 6

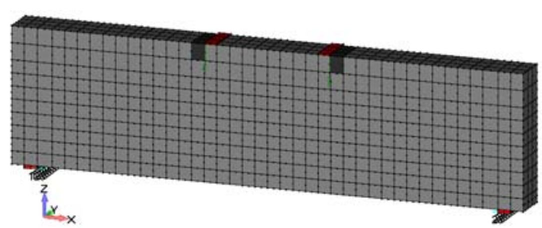

Group 7

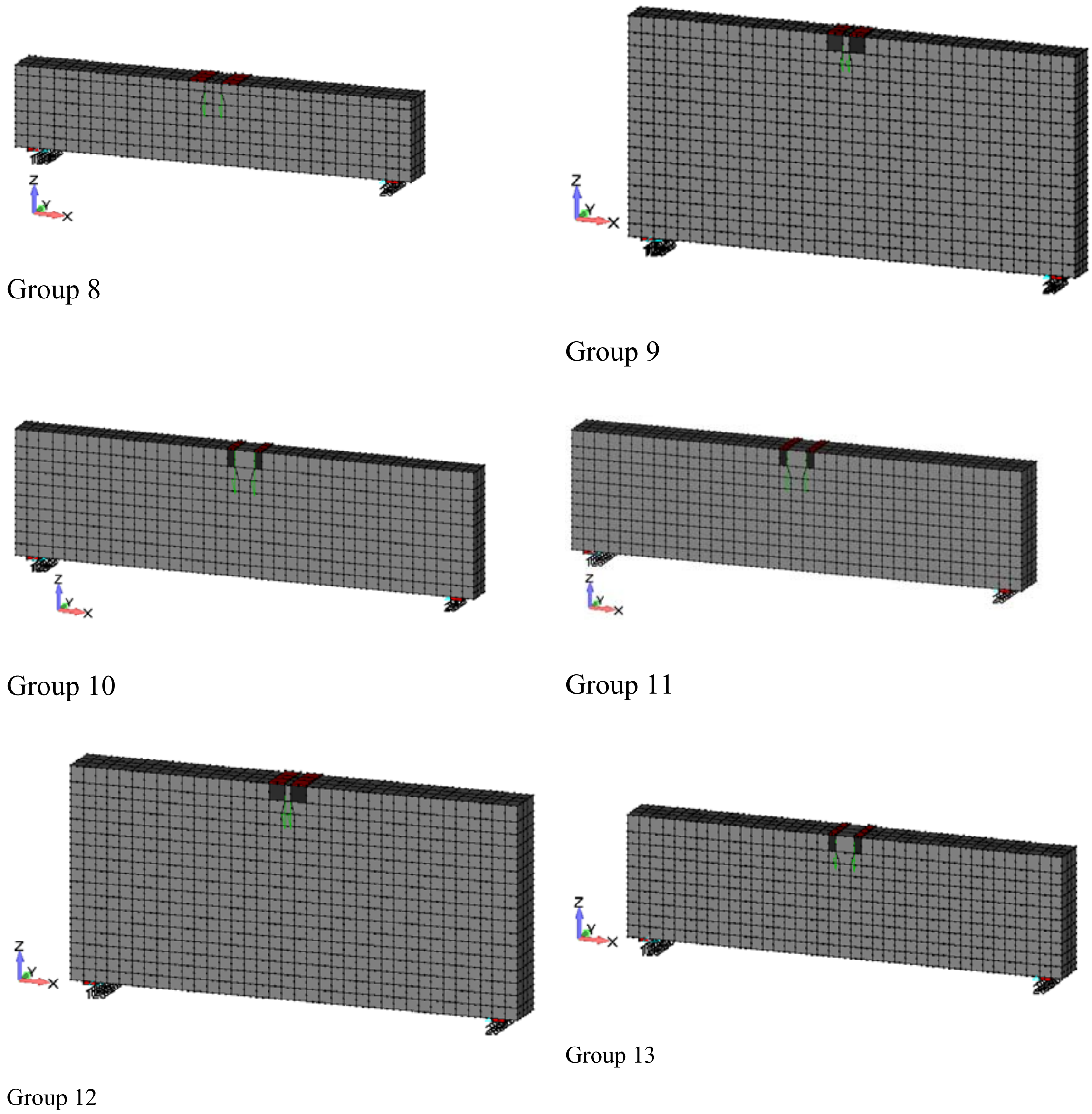

Figure 2 Hexahedral meshes for groups 1-13.

3.2 NLFEA Numerical Results

The development of the numerically derived load-deflection curves was performed on a standard 3.7 GHz personal computer (12 cores), where up to 5 models could be simultaneously analyzed. It is worth mentioning that the 93 models were successfully analyzed without any numerical instabilities. This has been consistently reported in previous published work, a finding that characterizes the stability and numerical robustness of the developed algorithm [50]–[55]. Fig. 3 shows the combined load-deflection curves a representative selection of the 84 FE models depicted in one figure for brevity and comparison purposes. The additional nine deep beams, which were included in the dataset used for training the proposed model, were analyzed in [50]. Based on the distribution of the curves obtained, it can be observed that the selected models represent a diverse spectrum of strength and stiffness values, providing a wide and densely populated spectrum of practical scenarios leading to a versatile approach with objectivity and applicability. The outcome of the NLFEA of the structural behavior of this type of RC deep beams will be further discussed in Section 4.

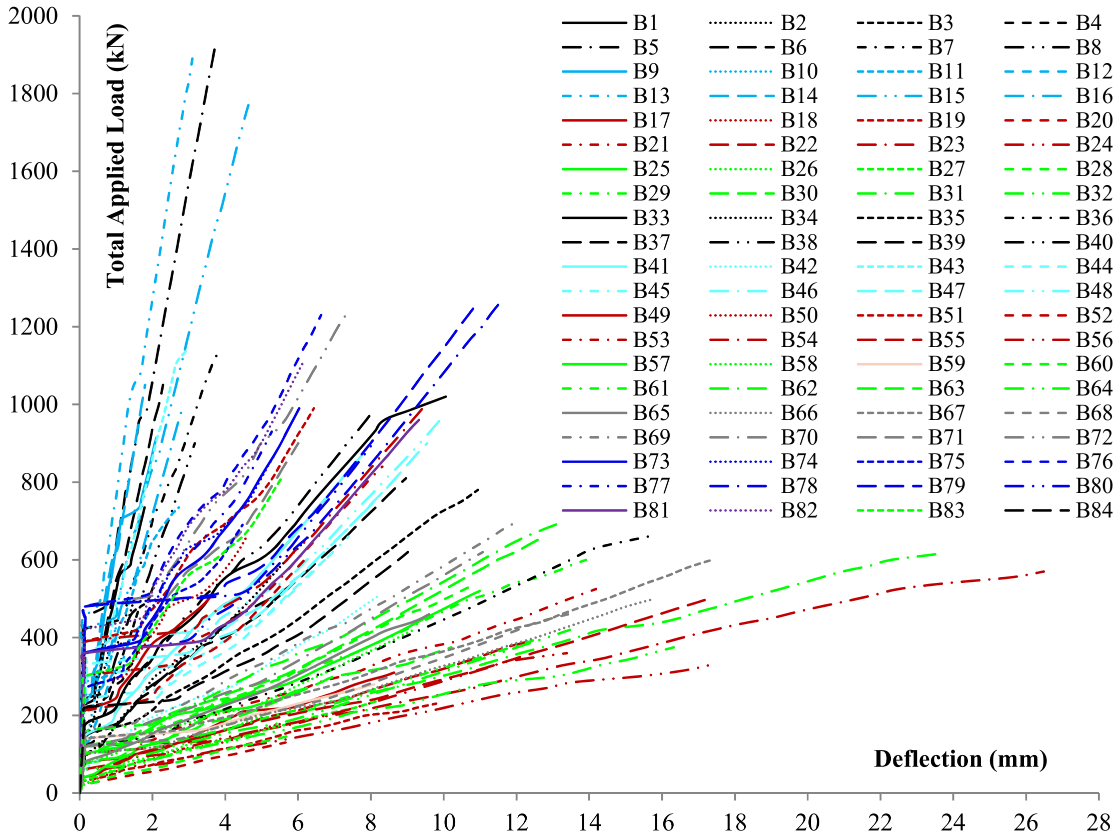

Figure 3 Load-Deflection curves of the 84 FE beam models.

4 AI-Model Development for Shear Capacity

Although computer experiments are very effective and economical than physical experiments involving the destructive testing of full-scale RC deep beams, they also suffer from increased cost and time constraints in complex simulations. Therefore, they can only afford a limited number of runs with a relatively large number of factors and are restricted to scarce sampling plans in investigating the mechanical response of structural response. ReConAn FEA [51] manages to overcome this limitation due to its optimum algorithmic design and the robust numerical response that efficiently addresses multiple analyses [37], [38]. Therefore, the generation of large databases can be feasible by replacing the physical experiment and developing design formulae, according to the problem at hand. This section will present the methodology of developing the proposed shear capacity model.

4.1 Descriptive Statistics

The input database consisted of nine variables in total, eight predictors, and one response, as presented in Table 3. As can be seen in Table 3, L is the span, b is the width, and d is the effective depth of the beams, where ρ is the reinforcement ratio, As is the reinforcement area and α/h is the shear span over the depth of the beam cross-section. The remaining variables refer to the material of concrete and FRP bars. Finally, the output refers to the maximum predicted capacity $V_{Rk,cp}$. The first step of the statistical investigation was the constitution of the histograms for both predictors and responses, and subsequently, the non-linear models were developed. The corresponding diagrams are presented in Figure 4, which demonstrate their variations.

Table 3. Input and response variables.

Input								Output
d	**b**	**L**	$\boldsymbol{a}$	f_c	f_{FRP}	ε_{FRP}	ρ	$V_{Rk,cp}$
(mm)	(mm)	(mm)	(mm)	(MPa)	(MPa)	(strains)	(%)	(kN)

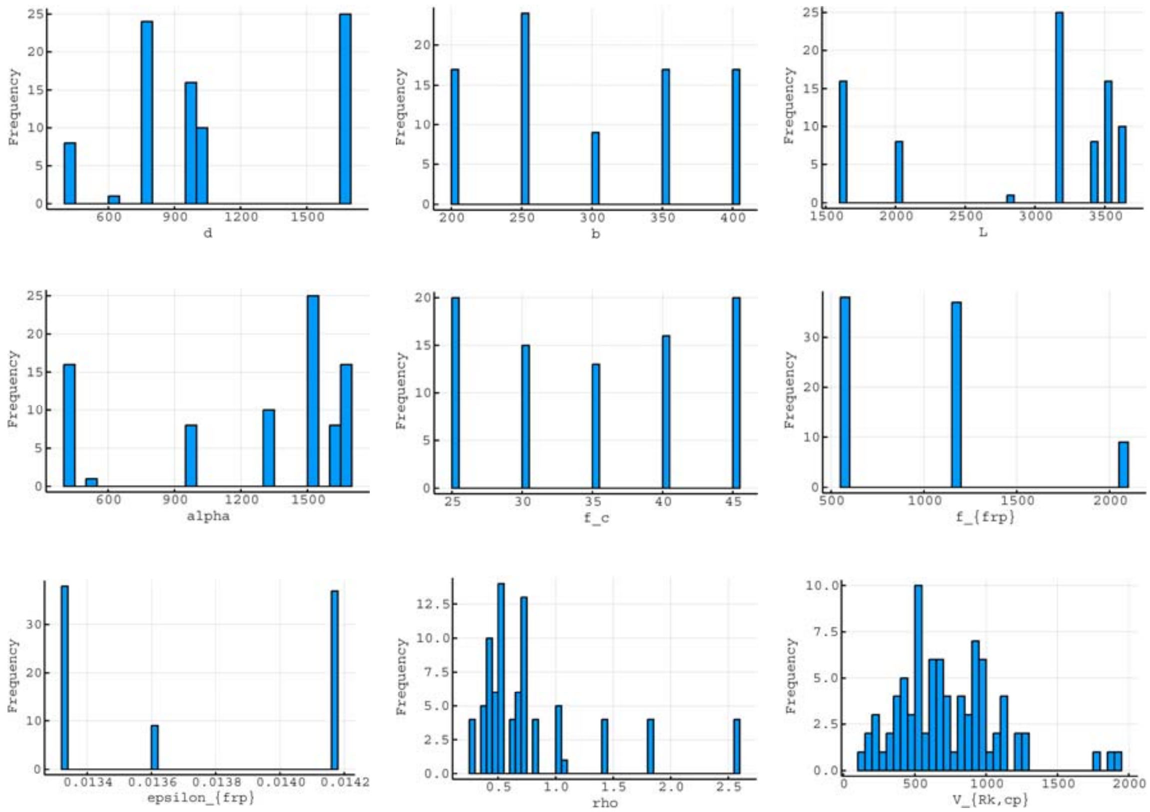

Figure 4 Histograms for input parameters.

4.2 Predictive Modeling

The raw database of 93 beams was utilized to train the ML models. To investigate the model's performance for testing on out-of-sample observations or blind predictions, 43 experimentally tested beams were used. Each variable $\mathbf{x}_i$ (predictors and response) was normalized by subtracting its mean value and dividing by its standard deviation, resulting in a new input variable $\mathbf{x}_i' = (\mathbf{x}_i - \overline{\mathbf{x}_i}) / \sigma(\mathbf{x}_i)$. Hence although the initial variables were of a different order of magnitude (i.e., modulus of elasticity vs. strains, etc.), the normalized variables had a mean value of zero and variance equal to the unity.

As described in [38], stepwise, nonlinear polynomial regression up to an order of three was implemented to constitute a prediction model. The nonlinear models considered the interactions among the variables, as well as remained easily interpretable by researchers and professional engineers. Five features were utilized, resulting in 18.6 observations per feature, to obtain statistically robust results. After the training of the model using Higher-Order Stepwise Regression (HOSR), the resulting equation was of the following form:

$$V_{Rk,cp} = 1.20 \cdot 10^{-4} f_c d b - 1.13 \cdot 10^{-5} a^2 f_c + 6.33 \cdot 10^{-6} f_{frp} f_c b - 1.47 \cdot 10^{-6} a b d + 9.42 \cdot 10^{-8} a^2 L + 115 \quad (4)$$

According to Table A in the appendix, all the variables within the developed formula are expressed in mm or N/mm^2, while the resulting characteristic shear capacity is computed in kN. This is an additional advantage of the adopted numerical approach in developing formulae, where the training can be performed by using the desired units for the input variables and selecting the required output variable units accordingly. Fig. 5 shows the correlation between the numerically generated characteristic shear strength $V_{Rk,cp}$ values and the predictions from the developed formula (Eq. 4). The E_c, E_{frp} were not used in the formula generation, as they are collinear with f_c, f_{frp} (auto-correlation coefficient = 0.99). This decision is necessary to avoid statistical instabilities in the model. The red lines indicate the acceptable range of shear values to check the reliability and validity of the proposed equation (Eq. 4) in comparison with the numerical results. The red lines indicate the +/- 95% confidence intervals.

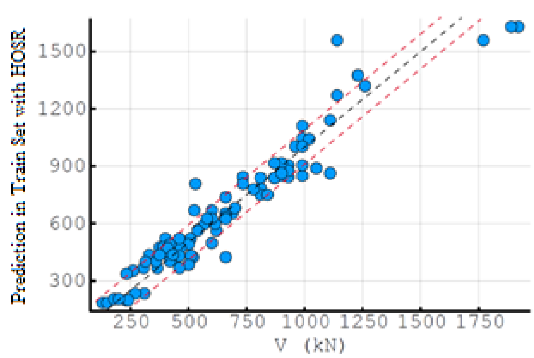

Figure 5 HOSR model shear strength prediction (Eq. 4) vs. NLFEA values.

4.3 Sensitivity Analysis

Three ML models were utilized to investigate the influence of each input parameter on the beam's structural response. The following AI modeling techniques were used: Linear Regression (LR), Higher-Order Stepwise Regression (HOSR), and Random Forests (RF) [55, 56]. The performance of each ML model for training and testing sets is demonstrated in Figure 6.

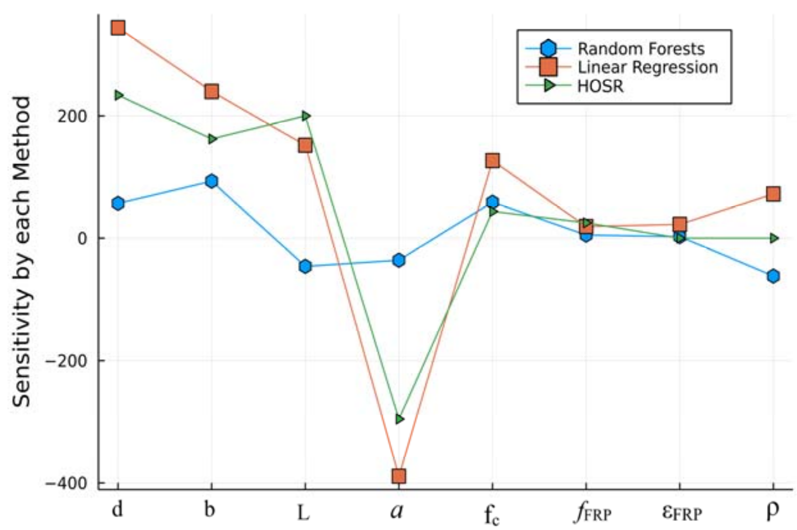

Figure 6 Input parameter sensitivity analysis using: Random Forest [58], Linear Regression [60], HOSR [70].

The predicted values were tested by utilizing the predicted values (PV), the dependent variable (DV), and the number of observations N, the metrics of the coefficient of dispersion (COD) as per (Eq. 5), the alpha metric (Eq. 6), the root mean squared error (RMSE) as shown in Eq. 7, the mean absolute error (MAE, Eq. 8), and the mean and maximum absolute percentage error (see Eqs. 9, 10). The Pearson correlation coefficient (Eq. 11), and the SR metric (Eq. 12) were also used herein.

The formulas for the computation of the metrics are defined as follows:

$$COD = 100 * \frac{\frac{1}{N}\Sigma(\left|\frac{PV}{DV}\right| - \frac{1}{N}\Sigma\frac{PV}{DV})}{\frac{1}{N}\Sigma\frac{PV}{DV}} \quad (5)$$

$$PV = Alpha * DV + Beta \quad (6)$$

$$RMSE = \sqrt{\frac{\Sigma(PV - DV)^2}{N}} \quad (7)$$

$$MAE = \frac{\Sigma|PV - DV|}{N} \quad (8)$$

$$MAPE = \frac{1}{N}\sum\frac{|PV - DV|}{DV} \quad (9)$$

$$MAXAPE = max(\frac{|PV - DV|}{DV}) \quad (10)$$

$$\rho_{X,Y} = \frac{cov(PV,DV)}{\sigma_{PV}\sigma_{DV}} \quad (11)$$

$$SR = \frac{PV}{DV} \quad (12)$$

The definitions of the metrics are presented in greater detail in [58], [59]. The analyses were conducted using MIT's Julia programming language [60] and previously developed computer codes in [61]. The results for each method are presented in Table 4. Figure 7 depicts the actual shear force, V versus the predicted Nonlinear Regression Model, exhibiting a clear linear association pattern. The red lines correspond to the MAE = 74.864 kN.

Table 4: Performance metrics (see Eqs 5-12)

	$\rho_{X,Y}$	MAE	RMSE	MAPE	MAXAPE	SR	Alpha	COD
RF	0.934	98.261	151.008	0.176	1.062	1.089	0.660	16.112
LR	0.924	97.184	136.687	0.181	1.225	1.008	0.853	17.798
HOSR	0.956	74.864	104.085	0.123	0.526	1.024	0.915	12.046

A modified version of the Profile method [62], [63] was applied to investigate each variable's influence on the output or the dependent variable. In particular, each input parameter was varied within its range in the raw dataset, while the other input parameters were retained constant at specific values. These specific values correspond to the Median (50% Percentile). The sensitivity analysis results of the proposed model are presented in Fig. 7.

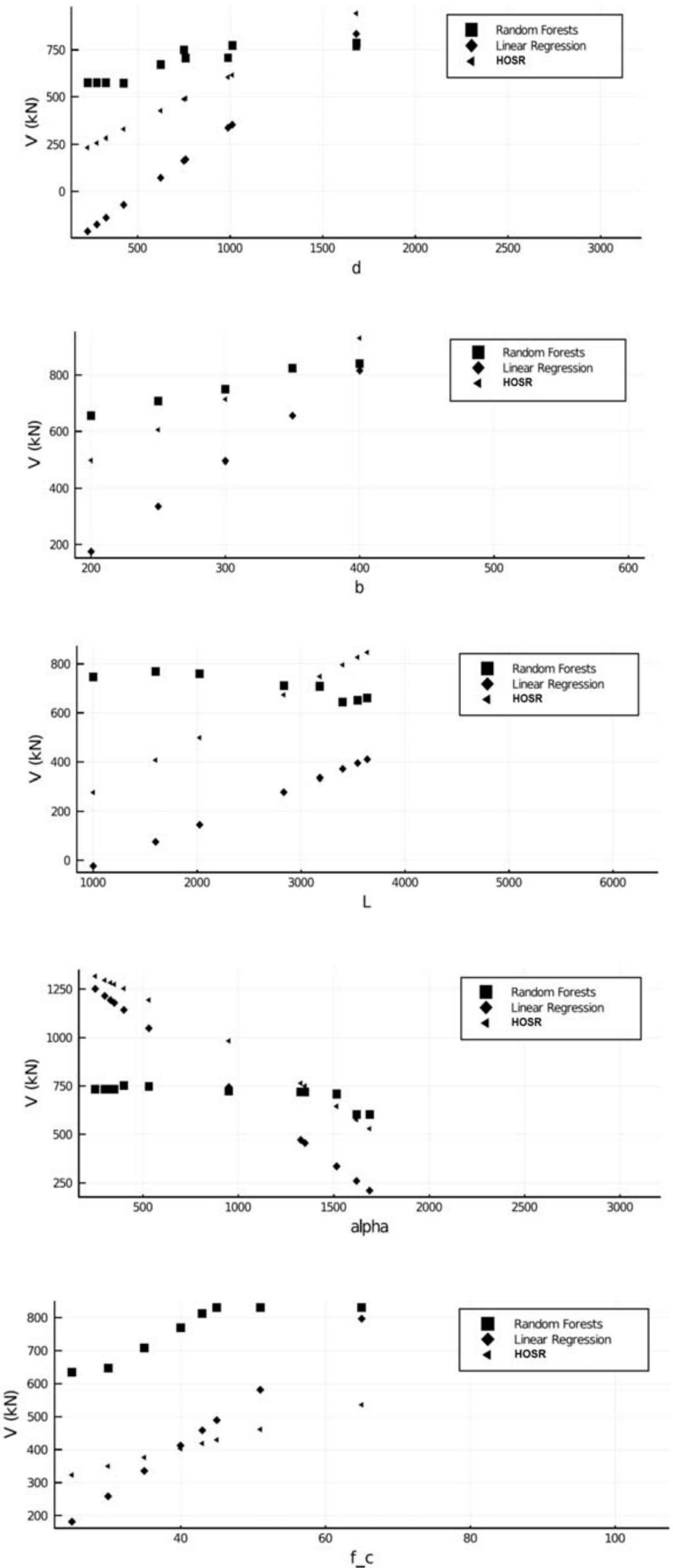
Random Forests
Linear Regression
HOSR
V (kN)
750
500
250
0
500
1000
1500
2000
2500
3000
d
Random Forests
Linear Regression
HOSR
V (kN)
800
600
400
200
200
300
400
500
600
b
Random Forests
Linear Regression
HOSR
V (kN)
800
600
400
200
0
1000
2000
3000
4000
5000
6000
L
Random Forests
Linear Regression
HOSR
V (kN)
1250
1000
750
500
250
500
1000
1500
2000
2500
3000
alpha
Random Forests
Linear Regression
HOSR
V (kN)
800
700
600
500
400
300
200
40
60
80
100
f_c

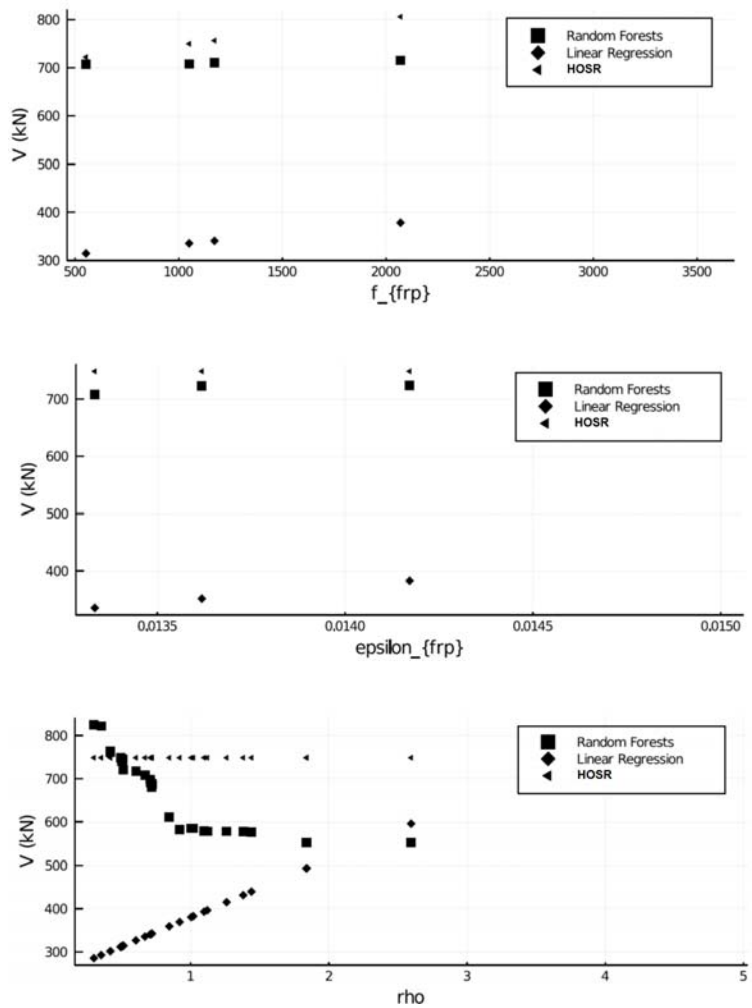

Figure 7 Sensitivity analysis for the significance of each predictor to the response.

A clear inverse relationship pattern between the shear strength and shear span a was identified. This could be attributed to the experimentally observed phenomenon of arching action, which typically vanishes as the shear span increases, since longer shear spans correspond to the flexure-dominated behavior of beams. Accordingly, the cross-sectional geometric characteristics of the beam (b and d) manifest high levels of influence on the shear capacity $V_{Rk,cp}$. The simpler model used, that is the linear regression (LR) model, suggests that the concrete uniaxial compressive strength f'_c correlates to increases in the shear strength of the deep beams. The ML models are in qualitative agreement; however, differences are attributed to the limited dataset. Hence, increasing the generated numerical results is a future research objective.

5 AI-Model Blind Prediction Comparison to EC and ACI codes

To benchmark the AI-generated model blind prediction capabilities proposed in Eq. 4, direct comparisons against the ACI 440.1R-15 and the Eurocode (EC) are carried out. Moreover, the AI-model was investigated against 43 experimentally tested beams (see Table 5). In the following sections, a brief demonstration of the design equations and conditions provided by each design code is presented.

Table 5: Data of the experimentally tested beams used for AI-model testing.

Data Source	ID	f_c (MPa)	E_c (MPa)	E_{FRP} (MPa)	f_{FRP} (MPa)	Failure Strain ε_{FRP} (mm/mm)	Reinf. Area (mm^2)	Reinf. Ratio ρ %	a/h	$V_{Rk,cp}$ (kN)
El-Sayed et al. [42]	94	39.4	29502	134000	986	0.0074	635.7	0.78	1.38	359
	95	40.5	29911	42000	749	0.0178	635.7	0.78	1.38	329
	96	39.4	29502	134000	986	0.0074	1010.6	1.24	1.38	390
	97	40.5	29911	42000	749	0.0178	1010.6	1.24	1.38	350
	98	39.4	29502	134000	986	0.0074	1393.65	1.71	1.38	467
	99	40.5	29911	42000	749	0.0178	1393.65	1.71	1.38	392
	100	39.4	29502	134000	986	0.0074	1010.6	1.24	1.06	744
	101	40.5	29911	42000	749	0.0178	1010.6	1.24	1.06	538
Kim et al. [34]	102	26.1	24011	80697	1827	0.0226	190	0.38	1.21	136
	103	26.1	24011	80697	1827	0.0226	190	0.38	1.47	99
	104	26.1	24011	80697	1827	0.0226	255	0.51	1.47	121
	105	26.1	24011	80697	1827	0.0226	320	0.64	1.47	134
	106	26.1	24011	80697	1827	0.0226	190	0.50	1.40	110

Data Source	ID	f_c (MPa)	E_c (MPa)	E_{FRP} (MPa)	f_{FRP} (MPa)	Failure Strain ε_{FRP} (mm/mm)	Reinf. Area (mm^2)	Reinf. Ratio ρ %	a/h	$V_{Rk,cp}$ (kN)
	107	26.1	24011	80697	1827	0.0226	316.2	0.51	1.51	134
	108	26.1	24011	120214	1956	0.0163	190	0.38	1.21	169
	109	26.1	24011	120214	1956	0.0163	190	0.38	1.47	107
	110	26.1	24011	120214	1956	0.0163	255	0.51	1.47	96
	111	26.1	24011	120214	1956	0.0163	320	0.64	1.47	151
	112	26.1	24011	120214	1956	0.0163	190	0.50	1.40	105
	113	26.1	24011	120214	1956	0.0163	316.2	0.51	1.51	145
Farghaly and Benmokrane [1]	114	49.3	33001	47600	790	0.0166	2270.79	0.69	1.04	1447
	115	49.3	33001	51900	750	0.0145	4047.36	1.24	1.04	1906
	116	38.7	29238	120000	1596	0.0133	866.58	0.26	1.04	1191
	117	38.7	29238	144000	1899	0.0132	1526.28	0.46	1.04	1601
Andermatt and Lubell [33]	118	40.2	29800	41100	709	0.0173	1187.083	1.49	0.90	814
	119	45.4	31668	41100	709	0.0173	1189.377	1.47	1.21	471
	120	40.5	29911	37900	765	0.0202	2565.3	1.70	0.89	1273
	121	39.9	29688	37900	765	0.0202	2570.13	1.71	1.22	799
	122	40.7	29984	41100	709	0.0173	3169.44	2.13	1.21	830
	123	66.4	38299	41100	709	0.0173	3160.92	2.12	1.21	1062
	124	51.6	33762	42300	938	0.0222	4227.9062	1.58	0.97	2269
	125	50.7	33466	42300	938	0.0222	4225.4784	1.56	1.32	1324

Data Source	ID	f_c (MPa)	E_c (MPa)	E_{FRP} (MPa)	f_{FRP} (MPa)	Failure Strain ε_{FRP} (mm/mm)	Reinf. Area (mm^2)	Reinf. Ratio ρ %	a/h	$V_{Rk,cp}$ (kN)
Nehdi et al. [64]	126	34.7	27686	134000	1180	0.0088	254.25	1.13	1.16	185
	127	38.9	29314	134000	1180	0.0088	254.25	1.13	1.37	155
	128	37.4	28743	134000	1180	0.0088	382.5	1.70	1.37	162
	129	39.6	29576	134000	1180	0.0088	508.5	2.26	1.37	186
	130	41.7	30351	134000	1180	0.0088	506.25	1.35	1.18	298
	131	63.1	37335	134000	1180	0.0088	254.25	1.13	1.37	227
	132	35.5	28003	40800	690	0.0169	290.25	1.29	1.16	136
	133	48.0	32563	40800	690	0.0169	290.25	1.29	1.37	129
	134	48.0	32563	40800	690	0.0169	384.75	1.71	1.37	147
	135	35.2	27885	40800	690	0.0169	519.75	2.31	1.37	122
	136	42.0	30459	40800	690	0.0169	521.25	1.39	1.18	243

5.1 Eurocode

According to Eurocode [20], in order to calculate the design resistance, $V_{Rd,c}$, of a particular section under shear due to the lack of stirrups in the concrete section, the following formula can be utilized:

$$V_{Rd,c} = [C_{Rd,c}\, k\, (\rho_l\, f_{ck})^{1/3} + k_1\, \sigma_{cp}]\, b_w\, d \qquad (13)$$

Where,

$C_{Rd,c} = 0.18 / \gamma_c$ is a semiempirical coefficient

$k = 1 + \sqrt{\frac{200}{d}} \leq 2.0$; (d in mm), is the size factor

$\rho_l = \frac{A_s}{b_w d} \leq 0.02$, is the longitudinal reinforcement ratio, where b_w is the smallest width of the cross-section in mm and d is the effective height of the cross-section in mm

f_{ck} is characteristic concrete compressive strength (MPa)

$\sigma_{cp} = \frac{N_{Ed}}{A_c} < 0.2 f_{cd}$ (MPa), where N_{Ed} is the axial force in the cross-section as a result of loading or prestressing, and A_C is the cross-sectional area of the concrete (mm^2)

The characteristic resistance of the section in shear can be calculated by setting the following recommended values: (1) the concrete material partial safety factor γc is set to 1, (2) $C_{Rd,c} = 0.18 / \gamma c$, and (3) $k_1 = 0.15$.

For the case where a concentrated load is applied near the support, Eurocode roughly approximates the shear resistance of the section. It estimates the design shear capacity for a shear span of a/d within the range of 0.5 to 2.0. Appropriate strength reduction is achieved through the parameter β = *a* / 2d, presented herein. The Eurocode does not mandate using the β parameter when a deep beam is designed for uniform loads. Whereas, in general, the design of a deep beam is often carried out as a structural member connecting columns to shear walls. For the purposes of this research work, this parameter is also investigated. Consequently, after computing the shear capacity of a section without stirrups, the characteristic shear resistance value per section will be divided by the β parameter ($V_{Rk,c}/\beta$). Additionally, it is important to note that the Eurocode 2 [20] formula is originally developed for steel and not GRFP reinforcement. As such, it is indicatively used herein for illustrative purposes.

5.2 ACI 318-14

According to ACI 318-14 [65], the nominal concrete shear strength V_c is given by Eq. (14). The equation is applicable for non-prestressed members with no axial forces. Otherwise, Table 6 shall be used to evaluate V_c.

$$V_c = (0.17\,\lambda \sqrt{f'_c})\, b_w\, d \qquad \text{SI units} \qquad (14)$$

$$V_c = (2\,\lambda\,\sqrt{f_c'})\,b_w\,d \qquad \text{US units}$$

Where λ is the modification factor to account for light-weight concrete, f_c' is the specified compressive strength of concrete (psi or MPa), b_w is the width of cross-section (in or mm), d is the distance from extreme compression fiber to centroid of tensile rebars (in or mm). Furthermore, ρ_w is the ratio of the area of non-prestressed longitudinal tension reinforcement A_s to $b_w d$, V_u is the factored shear force at the section (lb or N), M_u is the factored moment at the section (in-lb or N-mm). Table 6 shows the procedure of calculating V_c.

Table 6: Detailed procedure to calculate Vc [65], [66]

	V_c (SI units)	V_c (US units)
Least value obtained from the three equations	$\left(0.16\,\lambda\sqrt{f_c'} + 17\rho_w \frac{V_u d}{M_u}\right) b_w\,d$	$\left(1.9\,\lambda\sqrt{f_c'} + 2500\rho_w \frac{V_u d}{M_u}\right) b_w\,d$
	$\left(0.16\,\lambda\sqrt{f_c'} + 17\,\rho_w\right) b_w\,d$	$\left(1.9\,\lambda\sqrt{f_c'} + 2500\,\rho_w\right) b_w\,d$
	$0.29\,\lambda\sqrt{f_c'}\; b_w\,d$	$3.5\,\lambda\sqrt{f_c'}\; b_w\,d$

5.3 ACI 318-19

The new equations included in the ACI 318-19 [67] for calculating the concrete shear strength while considering their safety and performance aspects, are based on several factors. It was observed that the flexural reinforcement ratio along with the member depth are important parameters that have to be taken into consideration. It should be noted that the design equations do not account for the cases of shear walls and footings.

One-way shear

The concrete shear strength V_c shall be calculated using Eqs. (15) through (17).

$$V_c = \left(0.17\,\lambda\,\sqrt{f_c'} + \frac{N_u}{6\,A_g}\right) b_w\,d \qquad \text{SI units} \qquad (15)$$

$$V_c = \left(2\,\lambda\,\sqrt{f_c'} + \frac{N_u}{6\,A_g}\right) b_w\,d \qquad \text{US units}$$

$$V_c = \left(0.66\,\lambda\,(\rho_w)^{\frac{1}{3}}\,\sqrt{f_c'} + \frac{N_u}{6\,A_g}\right) b_w\,d \qquad \text{SI units} \qquad (16)$$

$$V_c = \left(8\,\lambda\,(\rho_w)^{\frac{1}{3}}\,\sqrt{f_c'} + \frac{N_u}{6\,A_g}\right) b_w\,d \qquad \text{US units}$$

$$V_c = \left(0.66\,\lambda_s\,\lambda\,(\rho_w)^{\frac{1}{3}}\,\sqrt{f_c'} + \frac{N_u}{6\,A_g}\right) b_w\,d \qquad \text{SI units} \qquad (17)$$

$$V_c = \left(8\,\lambda_s\,\lambda\,(\rho_w)^{\frac{1}{3}}\,\sqrt{f_c'} + \frac{N_u}{6\,A_g}\right) b_w\,d \qquad \text{US units}$$

Where N_u is the factored axial load (lb or N), A_g is the gross area of cross-section (in^2 or mm^2), ρ_w is the flexural reinforcement ratio, which is equal to $\frac{A_s}{b\,d}$, and λ_s is the size effect factor and is obtained by Eq. (18).

$$\lambda_s = \sqrt{\frac{2}{1 + 0.004\,d}} \leq 1 \qquad \text{SI units} \qquad (18)$$

$$\lambda_s = \sqrt{\frac{2}{1 + \frac{d}{10}}} \leq 1 \qquad \text{US units}$$

The selection of concrete shear strength equation(s) depends on the flexural and shear reinforcement areas. For members with shear reinforcement areas greater than the minimum specified by the code, the lesser outcome of Eq. (15) and Eq. (16) shall be used. However, for members with a shear reinforcement area less than the minimum, Eq. (17) will be used. Additionally, the concrete shear strength V_c for members of normal-weight concrete with no axial loads can be calculated using Eq. (19). The equation is only valid when a member has met the minimum shear reinforcement area specified by the code. It should be noted that the equation is the modification to Eq. (15).

$$V_c = \left(0.17\sqrt{f_c'}\right) b_w\, d \qquad \text{SI units} \qquad (19)$$

$$V_c = \left(2\sqrt{f_c'}\right) b_w\, d \qquad \text{US units}$$

Another condition was provided by the code, which states that V_c shall not be greater than a specific limit as follows:

$$V_c \le 0.42\, \lambda\sqrt{f_c'}\, b_w\, d \qquad \text{SI units} \qquad (20)$$

$$V_c \le 5\, \lambda\sqrt{f_c'}\, b_w\, d \qquad \text{US units}$$

5.4 ACI 440.1R-15

According to ACI 440.1R-15 [68], the procedure used to consider the effect of the axial stiffness of the FRP bars is by using the factor ([5 k / 2]), where k is defined as the ratio of the neutral axis depth to the reinforcement depth. The ACI 440.1R nominal concrete section shear capacity can be computed using:

$$V_c = \left(\frac{5}{2}k\right) 0.17\sqrt{f_c'}\, b_w d \qquad \text{SI units} \qquad (21)$$

$$V_c = \left(\frac{5}{2}k\right) 2\sqrt{f_c'}\, b_w d \qquad \text{US units}$$

Where,

f_c': compressive strength of concrete (psi/MPa)

$k = \sqrt{2\rho_f n_f + (\rho_f n_f)^2} - \rho_f n_f$.

n_f: ratio of modulus of elasticity of FRP bars to the modulus of elasticity of concrete

ρ_f: ratio of FRP reinforcement

5.5 Modified ACI 440.1R-15

The equations provided by both ACI 318-14 and ACI 318-19 cannot be used to calculate shear capacity for GFRP reinforced members since they have been derived for steel-reinforced members.

However, by tracing the changes adopted by ACI 318-19 to account for the size effects, a new expression could be derived for GFRP reinforced sections. Following the same concept adopted by ACI 440.1R-15 for considering the axial stiffness effects of the GFRP reinforcement, V_c is proposed to be calculated as follows:

$$V_c = \left(\frac{5}{2}k\right)\left(0.66\,\lambda_s\,\lambda\,(\rho_w)^{\frac{1}{3}}\sqrt{f_c'}\right)\,b_w\,d \qquad \text{SI units} \qquad (22)$$

$$V_c = \left(\frac{5}{2}k\right)\left(8\,\lambda_s\,\lambda\,(\rho_w)^{\frac{1}{3}}\sqrt{f_c'}\right)\,b_w\,d \qquad \text{US units}$$

With the condition

$$V_c \leq \left(\frac{5}{2}k\right)0.42\,\lambda\sqrt{f_c'}\,b_w\,d \qquad \text{SI units} \qquad (23)$$

$$V_c \leq \left(\frac{5}{2}k\right)5\,\lambda\sqrt{f_c'}\,b_w\,d \qquad \text{US units}$$

5.6 Comparison Results Between the Proposed AI-model and Design Codes

Figure 8 demonstrates the predictions (AI-model, ACI 440.1R-15, Modified ACI 440.1R-15, EC with β parameter) versus the NLFEA or experimentally obtained shear capacities. The EC case without β was omitted so as to avoid including a significantly large number of data points within the graph. The comparison reveals the following observations:

a. Based on the training and validation datasets that were used herein, the proposed AI-model demonstrates superior prediction and generalization capacity throughout the range of input parameters compared to the under-study design codes. To further emphasize this superior generalization capability of the AI-model, blind predictions were carried out on beams that are different from the 15% of input data, which was set aside to be used for testing purposes during the model development. The additional validation data for the blind predictions are obtained from the literature as summarized in Table 5 and represent physical experiments performed in laboratories. The generalization capabilities are demonstrated in Fig. 8 (when the AI-model is applied to new data). The average absolute error is 26% for the overall 136 samples and 57% for the blind predictions (43 samples). On average, the actual values are 99% of their corresponding predictions for the overall 136 samples and 93% for the blind predictions (43 samples). It is worth noting that the scatter of the AI-model predictions is also minimal.

b. The ACI 440.1R-15 predictions are relatively conservative compared to experiments and the calibrated high-fidelity NLFEA models. The ACI 440.1R-15 predictions are excessive and recommend major re-consideration and revision to the shear capacity evaluation approach. On average, the ACI 440.1R-15 code predictions are four times smaller than the actual values, and the absolute error is 77% on average. This could be attributed to the shear capacity calculation approach, which was originally developed for long shallow beams. Hence, this code is inherently incapable of capturing typical deep beam behavior (arching action, etc.). Such complex behavior is typically captured by more advanced methods, such as Strut-and-Tie models, where the deep beam is converted into an equivalent system of compression struts and tension ties.

c. The modified ACI 440.1R-15 predictions are lower than those calculated using the original version provided by the code, which yielded more conservative results. The predicted results are seven times smaller than the actual values, with an absolute error of 83% on average.

d. When applying the EC without the β parameter, the MAPE is 91% on the validation dataset (see Table 7), which is larger than that derived from the proposed model. Therefore, the proposed model that derived a 57% MAPE, is 34% more accurate than Eurocode, when estimating the shear strength of the 43 specimens. It is also important to note that about 53% of the blind prediction specimens (23 out of the 43) had smaller effective depths than the minimum depth used to develop the dataset that the AI model was extrapolated from (300 mm).

e. When the blind tests are performed on the specimens with geometries within the ranges used for the AI model development (shown in Table 1), the proposed formula derives a MAPE of 34%, while the EC without the use of β results in a MAPE of 91% (see Table 7), which represents about 268% of the proposed model prediction error. When using parameter β, EC blind predictions substantially improve, deriving a MAPE of 34% (10% increased error). Similarly, the two ACI equations (original and modified) derive a 77% and 83% MAPE, respectively. Moreover, when blind tests on the identical deep beams are performed (23 out of the 43), the MAPE increases by 224% and 254%, respectively. This finding further demonstrates the enhanced predictive characteristics of the proposed AI model. Even though the proposed AI-model predictions are shown to deliver a relatively small error, it is nevertheless a reliable source of input to be used for geometries within the ranges in Table 1.

f. The EC exhibits a significant improvement to the ACI 440.1R-15 predictions when the β parameter is adopted, with an MAPE of 36%, and average predictions that are 1.13 times less than their corresponding actual values. However, the EC predictions' scatter is quite large compared to the AI-model. Bearing in mind that the β parameter is applicable only for cases where a concentrated force is applied near the support, which is a rare occasion, especially when deep beams are used to connect columns to shear walls or in the case of pile caps.

It is worth mentioning that in Fig. 8c, where the prediction error is shown, the closer the points are to the dashed line, the smaller the overall error is achieved from the under-study method. The same applies for the case of Fig. 8d, where the actual over the predicted shear capacity is shown. It is easy to notice the superior predictive capabilities of the proposed equation that has the ability to capture the response derived from physically tested deep beams. Overall, the predictions of the AI-model outperform the design codes predictions when compared to new data sets (blind predictions). When the AI-model is compared to the NLFEA in terms of the computational effort, it is evident that the proposed model can provide predictions in milliseconds, whereas the NLFEA requires a relatively significant amount of time to setup and run high-fidelity numerical models. Further extensive blind prediction benchmarking is the objective of ongoing investigations to be included in future publications as extensions to this currently presented work. This is expected to revolutionize the current state of the art in RC structural design using FRP-reinforced and steel-reinforced concrete members for beams [70], slabs [71-73], and columns [74].

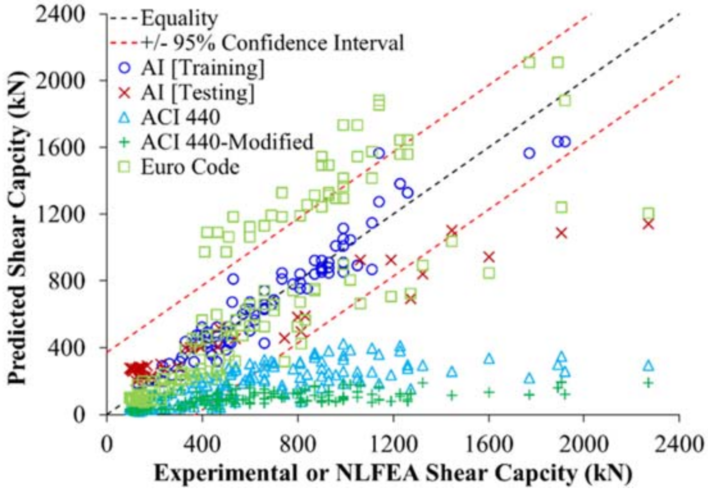
Equality
+/- 95% Confidence Interval
AI [Training]
AI [Testing]
ACI 440
ACI 440-Modified
Euro Code
Predicted Shear Capcity (kN)
Experimental or NLFEA Shear Capcity (kN)
0
400
800
1200
1600
2000
2400

(a)

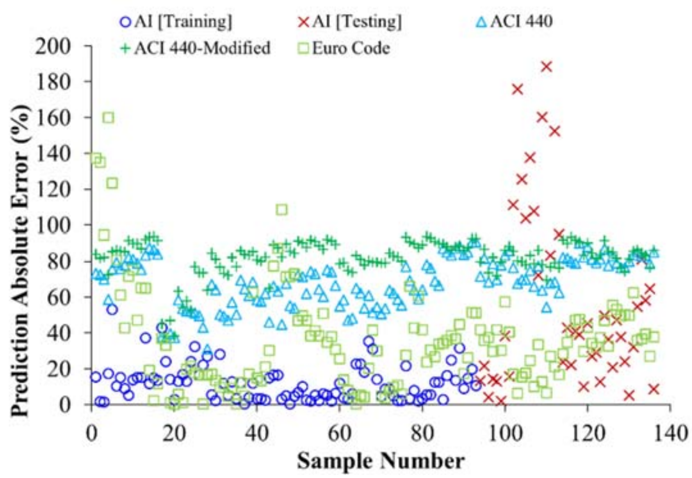
AI [Training]
AI [Testing]
ACI 440
ACI 440-Modified
Euro Code
Prediction Absolute Error (%)
Sample Number
0
20
40
60
80
100
120
140
160
180
200

(b)

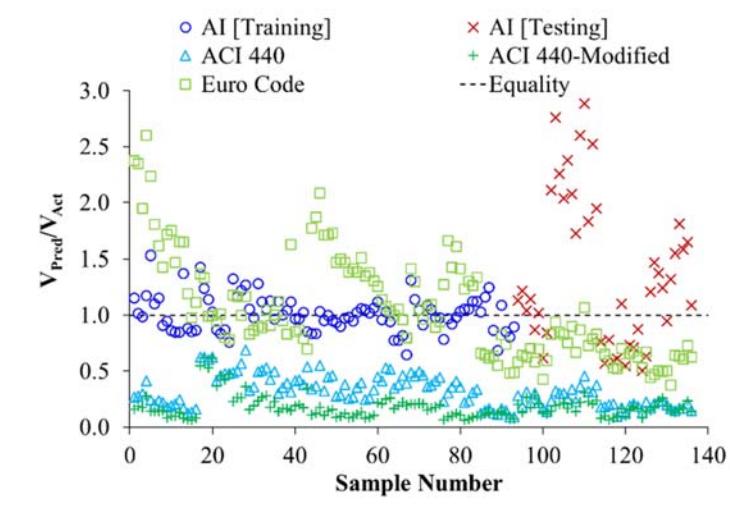
AI [Training]
AI [Testing]
ACI 440
ACI 440-Modified
Euro Code
Equality
V_{Pred}/V_{Act}
Sample Number
0.0
0.5
1.0
1.5
2.0
2.5
3.0
0
20
40
60
80
100
120
140

(c)

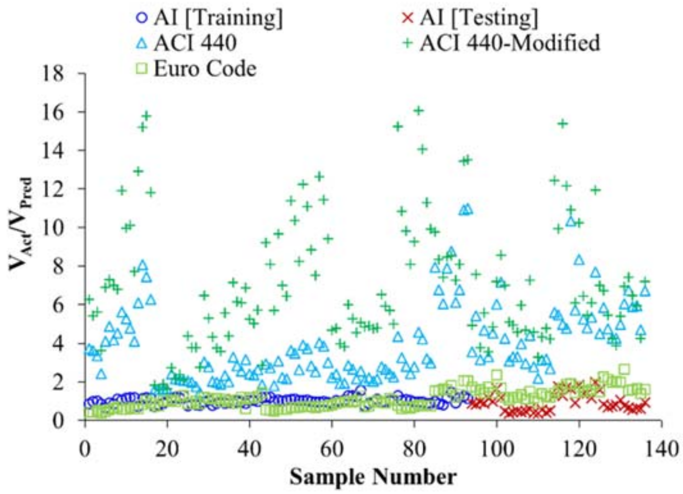

(d)

Figure 8 Prediction comparison of AI-model (HOSR), ACI, and EC with β codes: (a) Prediction comparison (b) Prediction error (c) Ratio V_{Pred}/V_{Act} (d) Ratio V_{Act}/V_{Pred}

Table 7: Mean average error on blind prediction beams depicted in Table 5

	AI	ACI 440	ACI 440-Modified	Eurocode without β	Eurocode with β
MAPE [%]	57	77	83	91	34
MAE [kN]	194	414	444	337	198

Concluding Remarks

The feasibility of developing AI-models to predict the shear strength of FRP-reinforced concrete deep beams was investigated herein through a novel pilot research study. To develop the AI-model, a set of data corresponding to 93 deep beams is used. A benchmark against several design standards was carried out, specifically: the EC, ACI 440.1R-15, and the modified ACI 440.1R-15 (for size effect). The blind predictions data comprised 43 beams that were experimentally tested previously and were obtained from the available literature.

Superior generalization capabilities were demonstrated by the proposed AI-model. The developed AI-model was shown to be an extremely cost-effective and non-computationally demanding tool for predicting the complex behavior of FRP-reinforced deep beams without shear reinforcement. The developed AI-model exhibits a number of advantages over the customary FEM methodology. In contrast to the FEM, the AI-model provides a closed-form mapping tool between input and output parameters. This allows for easier identification of influential inputs or combinations of inputs. The FEM procedure alone lacks any automatic adaptability or learning capabilities, which are essential assets for model generalization.

In FEM model discretization, the development of governing equilibrium equations and the solution of these equations, are all necessary steps for every possible combination of input parameters. In contrast, the AI-model is relatively much easier to develop, is immediately capable of predicting new data, and it can be updated to new input parameters and combinations. The ease of updating the proposed model, when new data is made available, further enhances the AI-model's capability of generalization. Other advantages of the AI-model are the relatively simpler architecture, feasibility of implementation, ease of reconfiguration, and above all, significantly faster simulation, which requires by orders of magnitude less computer effort. Furthermore, the relative simplicity of the derived expression qualifies it to be used in multi-objective optimization applications and lays the foundation for computing the key response parameters in future investigations.

According to the numerical investigation performed in this work, the Eurocode was found to enjoy the highest agreement with the experimental tests among the considered design codes and standards. The improvement to the predictions of shear capacities of deep beams reinforced with FRP bars could be attributed to the β parameter (indirectly accounting for the arching action effects).

Finally, further enhancements to the performance of the presented AI-models is to be expected in a future publication as a result of ongoing research efforts, where a more general shear capacity formula will be developed without the use of parameter α (shear span), along with the increase in the number of physical experiments being performed for validation purposes. A much more extensive data set is being prepared to represent larger variations of various deep beam configurations. The ongoing refinement of the AI-model shall enable much enhanced generalization capabilities for a variety of structural applications. The general distributed deep learning training methods that are currently being developed will provide superior AI-models with significantly improved predictive generalization capabilities.

6 Acknowledgment

The first author would like to express his appreciation for the continuous support provided by the Department of Civil Engineering, College of Engineering, American University of Sharjah (AUS). He would also like to extend his appreciation to the following individuals for their help and support during the execution of this research: Dr. Mahmoud Awad, Mr. Fouad Amin, Ms. Nouran Hegazy, Ms. Nour Ghazal Aswad, and Mr. Rami Zaher. This work received financial support by the EuroHPC-JU project EuroCC (G.A. 951732) of the European Commission. Parts of the runs were performed on the Cyclone machine hosted at the HPC National Competence Center of Cyprus at the Cyprus Institute (project pro21b103).

7 Data Availability

All models that support the findings of this study are available from the corresponding author upon reasonable request.

8 References

[1] A. S. Farghaly and B. Benmokrane, "Shear behavior of FRP-reinforced concrete deep beams without web reinforcement," *Journal of Composites for Construction*, vol. 17, no. 6, pp. 1–10, Dec. 2013.

[2] W. Ge *et al.*, "Experimental study on flexural behavior of ECC-concrete composite beams reinforced with FRP bars," *Composite Structures*, vol. 208, pp. 454–465, Jan. 2019.

[3] O. H. Zinkaah, A. Ashour, and T. Sheehan, “Experimental tests of two-span continuous concrete deep beams reinforced with GFRP bars and strut-and-tie method evaluation,” *Composite Structures*, vol. 216, pp. 112–126, 2019.

[4] G. Maranan, A. Manalo, B. Benmokrane, and W. M. Karunasena, “Shear behavior of geopolymer concrete beams reinforced with GFRP Bars,” *ACI Structural Journal*, vol. 114, no. 2, 2017.

[5] G. B. Maranan, A. C. Manalo, B. Benmokrane, W. Karunasena, P. Mendis, and T. Q. Nguyen, “Shear behaviour of geopolymer-concrete beams transversely reinforced with continuous rectangular GFRP composite spirals,” *Composite Structures*, vol. 187, pp. 454–465, 2018.

[6] H. Baghi, J. A. O. Barros, M. Kaszubska, and R. Kotynia, “Shear behavior of concrete beams reinforced exclusively with longitudinal glass fiber reinforced polymer bars : Analytical model,” *Structural Concrete*, vol. 19, no. 1, pp. 162-173., 2018.

[7] F. Abed, H. El-Chabib, and M. AlHamaydeh, “Shear characteristics of GFRP-reinforced concrete deep beams without web reinforcement,” *Journal of Reinforced Plastics and Composites*, vol. 31, no. 16, pp. 1063–1073, Aug. 2012.

[8] M. K. Dhahir, “Shear strength of FRP reinforced deep beams without web reinforcement,” *Composite Structures*, vol. 165, pp. 223–232, 2017.

[9] M. K. Dhahir, “Strut and tie modeling of deep beams shear strengthened with FRP laminates,” *Composite Structures*, vol. 193, pp. 247–259, 2018.

[10] ACI Committee 440, “Guide for the design and construction of concrete reinforced with FRP bars,” pp. 1–42, 2003.

[11] E. C. Bentz, L. Massam, and M. P. Collins, “Shear strength of large concrete members with FRP reinforcement,” *Journal of Composites for Construction*, vol. 14, no. 6, pp. 637–646, 2010.

[12] A. K. Tureyen and R. J. Frosch, “Shear tests of FRP-reinforced concrete beams without

stirrups," *ACI Structural Journal*, vol. 99, no. 4, pp. 427–434, Jul. 2002.

[13] D. Tomlinson and A. Fam, "Performance of concrete beams reinforced with basalt FRP for flexure and shear," *Journal of composites for construction*, vol. 19, no. 2, p. 04014036., 2015.

[14] Z. Omeman, M. Nehdi, and H. El-Chabib, "Experimental study on shear behavior of carbon-fiber-reinforced polymer reinforced concrete short beams without web reinforcement," *Canadian Journal of Civil Engineering*, vol. 35, no. 1, pp. 1–10, Jan. 2008.

[15] M. Guadagnini, K. Pilakoutas, and P. Waldron, "Shear resistance of FRP RC Beams : experimental study," *Journal of composites for construction*, vol. 10, no. 6, pp. 464–473, 2006.

[16] A. K. El-sayed and B. Benmokrane, "Shear strength of concrete beams reinforced with FRP bars : design method," *7th International Symposium on Fiber-Reinforced (FRP) Polymer Reinforcement for Concrete Structures*, pp. 955–974, 2005.

[17] ACI Committee 318, "Building code requirements for structural concrete and commentary (318 RM)," 2014.

[18] Canadian Standards Association, "Design of concrete structures (CSA A23.3-14)," 2014.

[19] A. K. El-sayed, E. F. El-salakawy, and B. Benmokrane, "Shear capacity of high-strength concrete beams reinforced with FRP bars," *ACI Structural Journal*, vol. 103, no. 3, p. 383, 2006.

[20] European Committee for Standardization, "Eurocode 2: design of concrete structures – part 1–1: general rules and rules for biddings.," 2015.

[21] K. H. Yang, H. S. Chung, E. T. Lee, and H. C. Eun, "Shear characteristics of high-strength concrete deep beams without shear reinforcements," *Engineering Structures*, vol. 25, no. 10, pp. 1343–1352, 2003.

[22] ASCE-ACI Committee 445, "Recent approaches to shear design of structural concrete," Farmington Hills, Michigan, USA, 1998.

[23] G. S. Harsha and P. P. Raju, “Shear strength of deep beams : a state of art,” *International Conference on Advances in Civil Engineering*, vol. 21, p. 23, 2019.

[24] R. L. Vollum and U. . Tay, “Strut and tie modelling of shear failure in short-span beams,” in *Concrete Communication Conference, UMIST, Manchester, British Cement Association/Concrete Society*, 2001, pp. 193–199.

[25] F. Vecchio and M. Collins, “The modified compression-field theory for reinforced concrete elements subjected to shear,” *ACI Journal Proceedings*, vol. 83, no. 2, pp. 219–231, 1986.

[26] Canadian Standards Association, “Design and construction of building components with fibre-reinforced polymers (CSA S806-12),” 2012.

[27] C. Arya, J. L. Clarke, and E. A. Kay, “TR 55: design guidance for stengthening concrete structures using fibre composite materials: a review,” *Engineering Structures*, vol. 24, no. 7, pp. 889–900, 2002.

[28] A. G. Razaqpur, B. O. Isgor, S. Greenaway, and A. Selley, “Concrete contribution to the shear Resistance of Fiber Reinforced Polymer Reinforced Concrete Members,” *Journal of Composites for Construction*, vol. 8, no. 5, pp. 452–460, Oct. 2004.

[29] S. P. Gross, D. W. Dinehart, J. R. Yost, and P. M. Theisz, “Experimental tests of high-strength concrete beams reinforced with CFRP bars,” in *Proceedings of the 4th International Conference on Advanced Composite Materials in Bridges and Structures (ACMBS-4), Calgary, Alberta, Canada (quoted from Razaqpur and Isgor, 2006)*, 2004.

[30] E. Shehata, “Fiber reinforced polymer (FRP) for shear reinforcement in concrete structures,” Ph.D. thesis, Department of Civil and Geological Engineering, University of Manitoba, 1999.

[31] A. K. El-Sayed, E. F. El-Salakawy, and B. Benmokrane, “Shear Strength of Reinforced Concrete Beams without Transverse Reinforcement,” *ACI Structural Journal*, vol. 103, no. 2, pp. 235–243, 2006.

[32] M. Said, M. A. Adam, A. A. Mahmoud, and A. S. Shanour, “Experimental and analytical shear

evaluation of concrete beams reinforced with glass fiber reinforced polymers bars," *Construction and Building Materials*, vol. 102, no. 3, pp. 574–591, 2016.

[33] M. F. Andermatt and A. S. Lubell, "Behavior of concrete deep beams reinforced with internal fiber-reinforced polymer-experimental study," *ACI Structural Journal*, vol. 110, no. 4, pp. 585–594, 2013.

[34] D. J. Kim, J. Lee, and Y. H. Lee, "Effectiveness factor of strut-and-tie model for concrete deep beams reinforced with FRP rebars," *Composites Part B: Engineering*, vol. 56, pp. 117–125, 2014.

[35] Canadian Standards Association, "Design and Construction of Building Components with Fibre-Reinforced Polymers (CSA S806-02)." p. 177, 2002.

[36] A. G. Razaqpur and O. B. Isgor, "Proposed Shear Design Method for FRP-Reinforced Concrete Members without Stirrups," *ACI Structural Journal*, vol. 103, no. 1, pp. 93–102, 2006.

[37] G. Markou and N. P. Bakas, "Artificial intelligence (A.I.) reinforced concrete: algorithms predict concrete strength without training on experimental data," *Innovate, University of Pretoria, South Africa*, 2019.

[38] G. Markou and N. P. Bakas, "Development of design formulae for the prediction of the shear capacity of reinforced concrete beams without shear reinforcement through the use of artificial intelligence algorithms," 2019.

[39] M. R. Islam, M. A. Mansur, and M. Maalej, "Shear strengthening of RC deep beams using externally bonded FRP systems," *Cement and Concrete Composites*, vol. 27, no. 3, pp. 413–420, 2005.

[40] T. El Maaddawy and S. Sherif, "FRP composites for shear strengthening of reinforced concrete deep beams with openings," *Composite Structures*, vol. 89, no. 1, pp. 60–69, 2009.

[41] N. Z. Hassan, A. G. Sherif, and A. H. Zamarawy, "Finite element analysis of reinforced

concrete beams with opening strengthened using FRP," *Ain Shams Engineering Journal*, 2015.

[42] A. K. El-Sayed, E. F. El-Salakawy, and B. Benmokrane, "Shear strength of fibre-reinforced polymer reinforced concrete deep beams without web reinforcement," *Canadian Journal of Civil Engineering*, vol. 39, no. 5, pp. 546–555, 2012.

[43] K. Mohamed, A. S. Farghaly, and B. Benmokrane, "Strut efficiency-based design for concrete deep beams reinforced with fiber-reinforced polymer bars," *ACI Structural Journal*, vol. 113, no. 4, pp. 791–800, 2016.

[44] H. Chen, W. Yi, and H. Hwang, "Cracking strut-and-tie model for shear strength evaluation of reinforced concrete deep beams," *Engineering Structures*, vol. 163, pp. 396–408, 2018.

[45] H. Chen, W. Yi, Z. John, and H. Hwang, "Modeling of shear mechanisms and strength of concrete deep beams reinforced with FRP bars," *Composite Structures*, vol. 234, p. 111715, 2020.

[46] M. F. Andermatt and A. S. Lubell, "Strength modeling of concrete deep beams reinforced with internal fiber-reinforced polymer," *ACI Structural Journal*, vol. 110, no. 4, p. 595, 2013.

[47] M. F. Andermatt and A. S. Lubell, "Strength Modeling of Concrete Deep Beams Reinforced with Internal Fiber-Reinforced Polymer," *ACI Structural Journal*, vol. 110, no. 4, pp. 595–606, 2013.

[48] I. M. Metwally, "Three-dimensional nonlinear finite element analysis of concrete deep beam reinforced with GFRP bars," *Housing & Building Research Centre (HBRC) Journal*, no. April, 2015.

[49] I. M. Metwally, "Three-dimensional nonlinear finite element analysis of concrete deep beam reinforced with GFRP bars," *Housing & Building Research Centre (HBRC) Journal*, vol. 13, no. 1, pp. 25–38, 2017.

[50] G. Markou and M. Alhamaydeh, "3D finite element modeling of GFRP-reinforced concrete deep beams without shear reinforcement," *International Journal of Computational Methods*,

vol. 15, no. 1, pp. 1–35, 2018.

[51] G. Markou, *ReConAn FEA Software User's Manual*. 2010.

[52] G. Markou and M. Papadrakakis, "Accurate and computationally efficient 3D finite element modeling of RC structures," *Computers and Concrete*, vol. 12, no. 4, pp. 443–498, 2013.

[53] G. Markou, M. Papadrakakis, and C. Mourlas, "Cyclic nonlinear analysis of large-scale finite element meshes through the use of hybrid modeling (HYMOD)," *International Journal of Mechanics*, vol. 11, no. 2017, pp. 218–225, 2017.

[54] G. Markou, C. Mourlas, and M. Papadrakakis, "A computationally efficient model for the cyclic behavior of reinforced concrete structural members," *Engineering Structures*, vol. 141, pp. 97–125, 2017.

[55] B. Sadeghi and Contributors, "DecisionTree.jl," GitHub repository. GitHub.

[56] Luis Pedro Coelho, "MILK: Machine Learning Toolkit - DecisionTree.jl." .

[57] L. Breiman, "Random Forests," *Machine learning*, vol. 45, no. 1, pp. 5–32, 2001.

[58] T. Dimopoulos and N. Bakas, "Artificial Intelligence for Mass Appraisals of Residential Properties in Nicosia: Mathematical Modelling and Algorithmic Implementation," in *Seventh International Conference on Remote Sensing and Geoinformation of the Environment*, 2019.

[59] T. Dimopoulos, H. Tyralis, N. P. Bakas, and D. Hadjimitsis, "Accuracy measurement of Random Forests and Linear Regression for mass appraisal models that estimate the prices of residential apartments in Nicosia, Cyprus," *Advances in Geosciences*, vol. 45, pp. 377–382, Nov. 2018.

[60] J. Bezanson, A. Edelman, S. Karpinski, and V. B. Shah, "Julia: A fresh approach to numerical computing," *SIAM review*, vol. 59, no. 1, pp. 65–98, 2017.

[61] N. P. Bakas, "NOESYS-AI Regression: A generic framework for predictive modeling and sensitivity analysis." 2018.

[62] J. D. Olden and D. A. Jackson, “Illuminating the ‘black box’: a randomization approach for understanding variable contributions in artificial neural networks,” *Ecological Modelling*, 2002.

[63] M. Gevrey, I. Dimopoulos, and S. Lek, “Review and comparison of methods to study the contribution of variables in artificial neural network models,” in *Ecological Modelling*, 2003.

[64] M. Nehdi, Z. Omeman, and H. El-Chabib, “Optimal efficiency factor in strut-and-tie model for FRP-reinforced concrete short beams with (1.5 < a/d < 2.5),” *Materials and Structures*, vol. 41, no. 10, pp. 1713–1727, Dec. 2008.

[65] C. 318 American Concrete Institute (ACI), “Building Code Requirements for Structural Concrete (ACI 318-14).” American Concrete Institute (ACI), Farmington Hills, MI, USA, 2014.

[66] ACI-318, *Building Code Requirements for Structural Concrete (ACI 318S-14) and Commentary (ACI 318SR-14)*. 2014.

[67] ACI Committee, *Building Code Requirements for Structural Concrete (ACI 318M-19)*. 2019.

[68] A. C. I. Committee, “ACI 440.1 R-15: guide for the design and construction of structural concrete reinforced with FRP bars,” *American Concrete Institute, Farmington Hills*, 2015.

[69] T. Dimopoulos and N. Bakas, “Sensitivity Analysis of Machine Learning Models for the Mass Appraisal of Real Estate. Case Study of Residential Units in Nicosia, Cyprus,” Remote Sens., vol. 11, no. 24, p. 3047, 2019, [Online]. Available: https://www.mdpi.com/2072-4292/11/24/3047.

[70] M.AlHamaydeh, F. Afghan, R. Mithani, T. Besiso, H. Al Salim, "Shear Strength of Circular Beams Made of Geopolymer Concrete and Reinforced with GFRP Rebars," Proceedings of the International Conference on Smart Sustainable Materials and Technologies (ICSSMT 2020), August 12-13, 2020, AIP Conference Proceedings 2297, 020031; https://doi.org/10.1063/5.0029862 .

[71] M. AlHamaydeh, M. Orabi, "Experimental Quantification of Punching Shear Capacity for Large-Scale GFRP-Reinforced Flat Slabs Made of Synthetic Fiber-Reinforced Self-Compacting Concrete Dataset," Data in Brief, Vol. 37, No. 5, August 2021, pp. 107196-6. DOI: 10.1016/j.dib.2021.107196.

[72] M. AlHamaydeh, M. Orabi, "Punching Shear Behavior of Synthetic Fiber-Reinforced Self-Consolidating Concrete Flat Slabs with GFRP Bars," ASCE, Journal of Composites for Construction, Vol. 25, No. 4, 2021, pp. 04021029-16, DOI: 10.1061/(ASCE)CC.1943-5614.0001131.

[73] M. AlHamaydeh, M. Orabi, M. Ahmed, S. Mohamed, A. Jabr, and M. K. Al Hariri, "Punching Shear Capacity of Macro Synthetic Fiber-Reinforced Concrete Two-Way Slabs with GFRP Rebars," Proceedings of the 11th International Conference on Composite Science and Technology (ICCST-11), pp. 75-80, Sharjah, UAE, April 4-6, 2017.

[74] M. AlHamaydeh, F. Amin, "Data for Interaction Diagrams of Geopolymer FRC Slender Columns with Double-Layer GFRP and Steel Reinforcement," Data, Vol. 6, No. 5, 2021, pp. 43-49. DOI:10.3390/data6050043.

9 Appendix A

Table A Input Parameters: Material and reinforcement details of the deep beam models, and FEA model Output: Maximum computed shear capacity.

	Input								Output
Model	f_c (MPa)	E_c (MPa)	E_{FRP} (MPa)	f_{FRP} (MPa)	Failure Strain, ε_{FRP} (mm/mm)	Reinf. Area As (mm^2)	Reinf. Ratio ρ %	a/h	$V_{Rk,cp}$ (kN)
01	25.0	23500	41400	552	0.013333	1528.2	1.02	0.50	410
02	25.0	23500	41400	552	0.013333	2159.6	1.44	0.50	465
03	25.0	23500	82700	1172	0.014172	1528.2	1.02	0.50	500
04	25.0	23500	82700	1172	0.014172	2159.6	1.44	0.50	420
05	45.0	31529	41400	552	0.013333	1528.2	1.02	0.50	530
06	45.0	31529	41400	552	0.013333	2159.6	1.44	0.50	735
07	45.0	31529	82700	1172	0.014172	1528.2	1.02	0.50	735

	Input								Output
Model	f_c (MPa)	E_c (MPa)	E_{FRP} (MPa)	f_{FRP} (MPa)	Failure Strain, ε_{FRP} (mm/mm)	Reinf. Area As (mm^2)	Reinf. Ratio ρ %	a/h	$V_{Rk,cp}$ (kN)
08	45.0	31529	82700	1172	0.014172	2159.6	1.44	0.50	930
09	25.0	23500	41400	552	0.013333	1528.2	0.51	0.50	900
10	25.0	23500	41400	552	0.013333	2159.7	0.72	0.50	990
11	25.0	23500	82700	1172	0.014172	1528.2	0.51	0.50	1050
12	25.0	23500	82700	1172	0.014172	2159.7	0.72	0.50	1050
13	45.0	31529	41400	552	0.013333	1528.2	0.51	0.50	1140
14	45.0	31529	41400	552	0.013333	2159.7	0.72	0.50	1770
15	45.0	31529	82700	1172	0.014172	1528.2	0.51	0.50	1920
16	45.0	31529	82700	1172	0.014172	2159.7	0.72	0.50	1890
17	25.0	23500	41400	552	0.013333	1560.9	1.84	2.00	130
18	25.0	23500	41400	552	0.013333	2205.8	2.60	2.00	150
19	25.0	23500	82700	1172	0.014172	1560.9	1.84	2.00	180
20	25.0	23500	82700	1172	0.014172	2205.8	2.60	2.00	200
21	45.0	31529	41400	552	0.013333	1560.9	1.84	2.00	230
22	45.0	31529	41400	552	0.013333	2205.8	2.60	2.00	240
23	45.0	31529	82700	1172	0.014172	1560.9	1.84	2.00	270
24	45.0	31529	82700	1172	0.014172	2205.8	2.60	2.00	310
25	25.0	23500	41400	552	0.013333	1527.6	0.50	2.00	330
26	25.0	23500	41400	552	0.013333	2158.9	0.71	2.00	375
27	25.0	23500	82700	1172	0.014172	1527.6	0.50	2.00	390
28	25.0	23500	82700	1172	0.014172	2158.9	0.71	2.00	375
29	45.0	31529	41400	552	0.013333	1527.6	0.50	2.00	570
30	45.0	31529	41400	552	0.013333	2158.9	0.71	2.00	615
31	45.0	31529	82700	1172	0.014172	1527.6	0.50	2.00	525
32	45.0	31529	82700	1172	0.014172	2158.9	0.71	2.00	600
33	35.0	27806	152000	2070	0.013618	2030.1	1.00	1.25	540
34	35.0	27806	152000	2070	0.013618	2030.1	0.50	1.25	990
35	25.0	23500	152000	2070	0.013618	2029.9	0.67	1.25	660
36	35.0	27806	41400	552	0.013333	2029.9	0.67	1.25	660
37	35.0	27806	82700	1172	0.014172	2029.9	0.67	1.25	780

	Input								Output
Model	f_c (MPa)	E_c (MPa)	E_{FRP} (MPa)	f_{FRP} (MPa)	Failure Strain, ε_{FRP} (mm/mm)	Reinf. Area As (mm^2)	Reinf. Ratio ρ %	a/h	$V_{Rk,cp}$ (kN)
38	35.0	27806	152000	2070	0.013618	1517.4	0.50	1.25	810
39	35.0	27806	152000	2070	0.013618	2029.9	0.67	0.50	1140
40	35.0	27806	152000	2070	0.013618	2029.9	0.67	1.25	870
41	35.0	27806	152000	2070	0.013618	2144.2	0.71	1.25	870
42	45.0	31529	152000	2070	0.013618	2029.9	0.67	1.25	1020
43	35.0	27806	152000	2070	0.013618	2055.8	1.10	2.00	510
44	25.0	23500	41400	552	0.013333	1759.5	0.42	0.88	600
45	25.0	23500	41400	552	0.013333	2070.5	0.49	0.88	600
46	25.0	23500	82700	1172	0.014172	1759.5	0.42	0.88	510
47	30.0	25743	41400	552	0.013333	1759.5	0.42	0.88	660
48	30.0	25743	82700	1172	0.014172	1760.0	0.42	0.88	660
49	30.0	25743	82700	1172	0.014172	2070.6	0.49	0.88	690
50	35.0	27806	41400	552	0.013333	1759.5	0.42	0.88	810
51	35.0	27806	41400	552	0.013333	2070.5	0.49	0.88	840
52	35.0	27806	82700	1172	0.014172	1759.5	0.42	0.88	810
53	40.0	29725	41400	552	0.013333	1759.5	0.42	0.88	900
54	40.0	29725	41400	552	0.013333	2070.6	0.49	0.88	930
55	40.0	29725	82700	1172	0.014172	1760.0	0.42	0.88	900
56	40.0	29725	82700	1172	0.014172	2070.6	0.49	0.88	870
57	45.0	31529	41400	552	0.013333	1759.5	0.42	0.88	960
58	45.0	31529	41400	552	0.013333	2070.5	0.49	0.88	990
59	45.0	31529	82700	1172	0.014172	1759.5	0.42	0.88	990
60	30.0	25743	41400	552	0.013333	1774.6	0.72	1.63	360
61	30.0	25743	41400	552	0.013333	2088.1	0.85	1.63	420
62	30.0	25743	82700	1172	0.014172	1774.6	0.72	1.63	420
63	30.0	25743	82700	1172	0.014172	2088.1	0.85	1.63	460
64	40.0	29725	41400	552	0.013333	1774.6	0.72	1.63	500
65	40.0	29725	41400	552	0.013333	2088.1	0.85	1.63	500
66	40.0	29725	82700	1172	0.014172	1774.6	0.72	1.63	520
67	40.0	29725	82700	1172	0.014172	2088.1	0.85	1.63	660

	Input								Output
Model	f_c (MPa)	E_c (MPa)	E_{FRP} (MPa)	f_{FRP} (MPa)	Failure Strain, ε_{FRP} (mm/mm)	Reinf. Area As (mm^2)	Reinf. Ratio ρ %	a/h	$V_{Rk,cp}$ (kN)
68	30.0	25743	41400	552	0.013333	1774.5	0.51	1.63	400
69	30.0	25743	41400	552	0.013333	2088.2	0.60	1.63	460
70	30.0	25743	82700	1172	0.014172	1774.5	0.51	1.63	540
71	30.0	25743	82700	1172	0.014172	2088.2	0.60	1.63	620
72	40.0	29725	41400	552	0.013333	1774.8	0.51	1.63	580
73	40.0	29725	41400	552	0.013333	2088.2	0.60	1.63	600
74	40.0	29725	82700	1172	0.014172	1774.5	0.51	1.63	700
75	40.0	29725	82700	1172	0.014172	2088.2	0.60	1.63	700
76	30.0	25743	41400	552	0.013333	1759.8	0.30	0.88	1110
77	30.0	25743	41400	552	0.013333	2070.4	0.35	0.88	900
78	30.0	25743	82700	1172	0.014172	1759.8	0.30	0.88	990
79	30.0	25743	82700	1172	0.014172	2070.4	0.35	0.88	930
80	35.0	27806	82700	1172	0.014172	2070.4	0.35	0.88	1110
81	40.0	29725	41400	552	0.013333	1759.8	0.30	0.88	1260
82	40.0	29725	41400	552	0.013333	2070.4	0.35	0.88	1260
83	40.0	29725	82700	1172	0.014172	1759.8	0.30	0.88	1230
84	40.0	29725	82700	1172	0.014172	2070.4	0.35	0.88	1230
85	34.4	27566	51000	1050	0.020588	423.2	0.92	0.83	307
86	34.4	27566	51000	1050	0.020588	423.2	0.92	1.00	262
87	34.4	27566	51000	1050	0.020588	423.2	0.92	1.17	233
88	34.4	27566	51000	1050	0.020588	634.8	1.38	0.83	366
89	34.4	27566	51000	1050	0.020588	846.4	1.84	0.83	461
90	34.4	27566	51000	1050	0.020588	627.2	1.12	0.83	315
91	34.4	27566	51000	1050	0.020588	831.6	1.26	0.83	433
92	40.8	30021	51000	1050	0.020588	423.2	0.92	0.83	442
93	52.0	33892	51000	1050	0.020588	423.2	0.92	0.83	475